

264196
RTA

PHIL. TRANS. R. SOC. LOND. A COPY

C.U.P. expect blocks by 14 May 76

c.v.p. to set, make blocks for figures 7, 14, 16: copy checked

A.9

The breakdown of superfluidity in liquid ^4He :
an experimental test of Landau's theory

169-14
CA

some chem
elements

Supply
Xerox copies of
a/w for
checking

169-11
CA

By D.R. Allum, P.V.E. McClintock and A. Phillips,

Department of Physics,

University of Lancaster,

Lancaster,

and

R.M. Bowley,

Department of Physics,

The University,

Nottingham.

(Communicated by W.F. Vinen, F.R.S. - Received
13 January 1976)

Notes: pagination runs straight through, except:

... 35, 36a, 36b, 36c, 37, ...

and ... 49, 50a, 50b, 51 ...

9

Marked-up typescript of paper published in
Phil. Trans. R. Soc. Lond A 284, 179-224 (1977).

() () () ()
Contents

PAGE

text
type

✓ 1. Introduction

- ✓ (a) Landau's explanation of superfluidity in ^4He 3 000
- ✓ (b) Measurements of the critical velocity. 6 000
- ✓ (c) Ion motion in pressurized superfluid ^4He . 8 000
- ✓ (d) Field emission in superfluid ^4He . 10 000

✓ 2. Apparatus and techniques

- ✓ (a) The single-pulse time-of-flight technique. 13 000
- ✓ (b) The experimental chamber. 15
- ✓ (c) Electrical circuit. 16
- ✓ (d) Cryogenics. 19

✓ 3. Experimental results

- ✓ (a) Velocity measurements. 21
- ✓ (b) Signal magnitudes. 24
- ✓ (c) Accuracy. 27

✓ 4. Discussion

- ✓ (a) Comparison with Landau's theory. 29
- ✓ (b) The failure of Takken's theory. 30
- ✓ (c) Critical energy dissipation by a light object. 31
- ✓ (d) Supercritical energy dissipation : single-roton emission. 35
- ✓ (e) Supercritical energy dissipation : two-roton emission. 41
- ✓ (f) ^{Is} Absence of the single-roton process? *forbidden* 51

✓ 5. Conclusion

Appendix A: Tabular velocity data 57

Appendix B: The single-roton transition rate 64

cont.

see over

*continuation
of contents*

Appendix ^CIN : The two-roton transition rate

66 000

Appendix ^DIV : Glossary of symbols

70 000

References

77 000

127
solid
non chem
elements
stable symbols
slip greek
unless otherwise
indicated
NB
127

← A single pulse time of flight technique has been used to determine the drift velocity \bar{v} of the negative ions injected into liquid ⁴He from a field emission source. Measurements of \bar{v} as a function of temperature T , pressure P and electric field E are presented within the range: $0.29 \leq T \leq 0.5K$; $21 \times 10^5 \leq P \leq 25 \times 10^5$ Pa; $1 \leq E \leq 300$ kV m⁻¹. The experimental results are in good agreement with Landau's theory of superfluidity. The data are used to demonstrate the inapplicability of two theories of supercritical dissipation: by Takken, based on an assumption of coherent roton emission; and by Bowley & Sheard, based on the assumption of incoherent single-roton emission. The results are, however, shown to be in excellent agreement with Bowley & Sheard's incoherent two-roton theory, and the data are used to derive a numerical value of the matrix element characterizing two-roton emission. The surprising absence of the single-roton emission process is discussed, and an upper bound is placed on the relevant matrix element.

127
127

1. Introduction

← Superfluidity is the most remarkable of the properties of liquid ⁴He. The only other systems known to exhibit comparable behaviour are the liquid phase of the other stable isotope of helium, ³He, and the electron gas in a superconducting metal; it is believed that the nucleonic fluids in a neutron star may also be superfluid, but this is less certain because data inevitably are scanty. Superfluidity implies the possibility of non-dissipative flow of the fluid through a channel or, conversely, that an object may be able to move through the stationary fluid without experiencing any viscous drag.

At temperatures well below that of its superfluid transition (2.18K at s.v.p.), which in practice usually means $T < 1.0\text{K}$, liquid ⁴He behaves as a superfluid in which there exists a dilute gas of particle-like elementary excitations. The superfluid has zero entropy and has zero viscosity, all the thermal energy of the liquid being carried by the excitation gas. An object moving through the liquid will therefore encounter a slight resistance owing to its scattering of elementary excitations, but no resistance at all from the superfluid itself. The residual drag caused by the excitation gas will, of course, fall rapidly with temperature as the excitation density decreases.

By employing simple arguments based on considerations of the conservation of energy and momentum, Landau (1941, 1947) was able to account for the superfluidity of ⁴He in

terms of the shape of the dispersion curve for the elementary excitations. As discussed in § 1(a) below, a fundamental prediction of his theory is that there will be a well-defined critical velocity above which the superfluidity will disappear and dissipative behaviour will be observed. The main objective of the present work was to test this prediction by measuring, as a function of their velocity, the drag experienced by negative ions travelling through superfluid ^4He below 0.5K, and thus to achieve an accurate experimental determination of the Landau critical velocity v_L .

In § 1(b) we review very briefly the outcome of earlier attempts to measure the critical velocity, and the reasons why they failed to yield experimental values of v_L . We discuss in § 1(c) the motion of negative ions through pressurized superfluid ^4He , and we indicate why this particular experimental situation appeared to offer a unique opportunity to test both Landau's theory and the subsequent supercritical drag calculations of Takken (1970); and we describe the unexpected failure of experiments with these purposes in view. More recently, however, it has been found that field emission characteristics in superfluid ^4He display certain anomalous features when pressure is applied to the liquid, and in § 1(d) we indicate why these phenomena seemed to imply the feasibility of the present research programme based on the use of field emission ion sources.

stat. & sloping except where shown

centre

(a) Landau's explanation of superfluidity in ^4He

We consider, as sketched in figure 1, an object of mass m travelling with initial velocity v_e through a motionless fluid. Its kinetic energy can be reduced if it creates in the fluid an excitation of energy ϵ and momentum $\hbar k$, so that it travels finally with the smaller velocity v_f . In order that energy and momentum be conserved in the process,

Figure 1

- bold ital
bar with h
from f e

$$\frac{1}{2} m v_e^2 = \frac{1}{2} m v_f^2 + \epsilon \quad (1)$$

and

$$m v_e = m v_f + \hbar k \quad (2)$$

Eliminating v_f between (1) and (2),

mid pt raised on pt

$$\frac{1}{2} m v_e^2 = \frac{1}{2} m (v_e^2 - 2 \hbar k \cdot v_e + \hbar^2 k^2 / m^2) + \epsilon$$

from cos

giving

$$v_e \cos \theta = \epsilon / \hbar k + \hbar k / 2m$$

where θ is the angle between v_f and k . Because $\cos \theta \leq 1$, we conclude that

$$v_e \geq \epsilon / \hbar k + \hbar k / 2m$$

Unless this condition is fulfilled it will be impossible simultaneously to satisfy the requirements for conservation of energy and momentum. There will consequently be a critical initial velocity of the object

prime
from min

$$v' = (\epsilon / \hbar k + \hbar k / 2m)_{\min} \quad (3)$$



below which the creation of excitations, and thus the dissipation of its kinetic energy, cannot occur. It is conventionally assumed that the second term is negligible compared to the first (but we shall return to consider this question in more detail in § 4(b)), so that the Landau critical velocity,

$$v_L = (\epsilon/\hbar k)_{\min} \quad (4)$$

Whether or not a given liquid will be superfluid must therefore depend on whether or not v_L is non-zero, and this in turn will depend on the form of $\epsilon(k)$. The thermal energy of ordinary liquids occurs as the kinetic energy of individual atoms or molecules, so that $\epsilon = \hbar^2 k^2 / 2m$ and hence $(\epsilon/\hbar k)_{\min} = 0$. In superfluid helium, on the other hand, it is not meaningful to refer to the kinetic energy of any individual atom: the thermal energy is carried by elementary excitations which have the energy momentum relationship shown in figure 2 (which illustrates the situation where the liquid is held close to its solidification pressure: this was always the case in the experiments to be described below). This curious dispersion curve, the form of which was originally predicted by Landau (1941, 1947) and which has since been verified in numerous experiments, is thus responsible for the superfluidity of liquid ^4He in that it quite evidently determines that $\epsilon/\hbar k$ should nowhere be zero.

The smallest value of $\epsilon/\hbar k$ clearly lies near the minimum of the curve in the region where the excitations are known as rotons and where, to a good approximation,

from L
throat

Figure 2

bar
with \hbar



sloping
-5-

please note upright delta used later, p. 31

$$\epsilon = \Delta + \hbar^2 (k - k_0)^2 / 2m_r \quad (5)$$

Here Δ , k_0 and m_r , which are known as the Landau roton parameters and are weakly pressure dependent, specify respectively the energy, momentum and effective mass of a roton at the minimum. To find $(\epsilon/\hbar k)_{\min}$, we set

$$\frac{d}{dk} (\epsilon/\hbar k) = 0,$$

yielding

$$\frac{d\epsilon}{dk} = \epsilon/k \quad (6)$$

Substituting for ϵ from (5) we can then determine the value of k which makes $\epsilon/\hbar k$ a minimum and thence, using (4) and (5), we can determine v_L precisely. For most purposes, however, a simpler approach suffices. We note that (6) implies that v_L is specified by the gradient of a line drawn from the origin to make a tangent with the roton region of the curve, contacting it very close to the minimum at (Δ, k_0) , as indicated in figure 2. In fact

$$v_L \approx \Delta/\hbar k_0 \quad (7)$$

within 1%. Inserting experimental values of Δ and k_0 (Donnelly (1972)), we find that $v_L = 58 \text{ ms}^{-1}$ at s.v.p, and $v_L = 46 \text{ ms}^{-1}$ close to the solidification pressure at $25 \times 10^5 \text{ Pa}$.

Thus, at low temperatures where the drag caused by the scattering of thermal excitations is negligible, which in practice usually means $T < 0.5K$, the drag on an object moving through He II should vary with its velocity as indicated in figure 3. The drag will remain zero until the critical velocity v_L is attained, and then dissipation will set in

Figure 3

very abruptly. Similar arguments may, of course, be applied to the case of superfluid helium moving through a tube showing that, for velocities less than v_L , there should be no viscous resistance to flow.

(b) Measurements of the critical velocity

A very large number of superflow experiments which test the predictions of Landau's theory have been carried out, and extensive accounts are given in the various standard texts on liquid helium such as those by Wilks (1967) and Keller (1969). Critical velocities have indeed been observed and measured for helium flowing in a wide variety of geometries including capillary tubes, adsorbed films and tightly packed powders. In every case, however, the experimental value of the critical velocity was orders of magnitude smaller than v_L , typically being no more than a few $\frac{\text{millimetres per second}}{\text{mm}} \text{ s}^{-1}$. Recently, Harrison & Mendelssohn (1974) and Hess (1974) reported critical flow velocities of up to 7 m s^{-1} through the tiny ($\approx 20 \text{ nm}$) holes formed by etching irradiated mica, but even this is smaller by a factor of about eight than the value predicted by Landau. The low critical velocities observed experimentally have mostly been attributed to complications arising from the production of turbulence in the superfluid, the possible existence of which we ignored in § 1(a). A certain minimum flow velocity, dependent on the channel dimensions, is again required and, apparently because the critical velocity for the creation of quantised vortices is much smaller than v_L , the breakdown

of superfluidity through Landau's roton creation mechanism has never been observed in a flow experiment.

The other possible experimental approach is, of course, that depicted in figure 1 : to move an object through stationary superfluid. Negative and positive ions constitute particularly convenient objects for this purpose. They can readily be injected into the liquid ^{by means of} ~~using~~ a variety of different techniques, they can be moved through the liquid by application of electric fields, and their arrival at an electrode can be observed as a pulse of current. The so-called ions which can exist in liquid helium are, in fact semi-macroscopic objects with radii of ^{ca. # nm} $\sim 1\text{nm}$ and effective masses of ^{ca.} $\sim 100m_4$, where m_4 ^{is} the mass of a ${}^4\text{He}$ atom. Numerous investigations of ion motion in liquid ${}^4\text{He}$ have been carried out, and have been reviewed, with extensive bibliographies, by Fetter (1975) ^{os.} and by Schwarz (1975). In such experiments it has been found that, as the electric field is increased from zero, the drift velocity of the ion, which is limited by the scattering of thermal excitations, also at first increases; but in almost every case, at a critical velocity of ^{ca. #} $\sim 30\text{m s}^{-1}$ the bare ion undergoes a transition to a charged vortex state and, thereafter, the velocity of the complex falls with increasing electric field in precisely the manner expected of a vortex ring. Such experiments have been extremely rewarding and have led, for example, to accurate measurements of the quantum of circulation. Because the bare-ion to charged-
vortex-ring transition can usually be characterized by a

critical velocity which is less than v_L the experiments have not, however, enabled any satisfactory test of Landau's roton emission theory to be carried out. The only exception seems to be in the particular case of negative ions moving through liquid helium under pressure.

(c) Motion of negative ions in pressurized He II

Meyer and Reif (1961) reported that the behaviour of negative ions in pressurized He II was quite different from that of positive ions, or of negative ions at lower pressures, in that for temperatures near 0.6K it was possible to accelerate them to velocities of 50-60ms⁻¹. This was later confirmed by Rayfield (1966, 1968). He found that for $P > 12 \times 10^5$ Pa (10^5 Pa \approx 1 bar) it was possible to accelerate negative ions to velocities approximating to v_L ; he deduced that in his highest electric fields of 7kV m⁻¹ the ions were approaching a limiting velocity; and he concluded that this apparent limiting velocity rose as the pressure was reduced. The latter was precisely the behaviour expected of v_L : $\Delta/\hbar k$ increases with a decrease in pressure, owing to changes in the shape of the excitation spectrum. Unfortunately, Rayfield's experiment was at a temperature, 0.6K, where drag on the ions owing to excitation scattering was considerable and it was not, therefore, possible to be entirely sure that true critical velocity behaviour was being observed, or to measure the component of the drag arising from excitation creation as opposed to that arising from scattering.

new

The simple approach suggested by Landau did not, of course, make any prediction about the magnitude of the drag which would be experienced by an object travelling faster than v_L : Landau demonstrated merely that there would be no drag at all from the superfluid at lower velocities so that, for example, any of the three curves sketched in figure 3 would be equally consistent with his theory.

The first ^{detailed} calculation of the drag on an object travelling at supercritical velocities seems to have been that by Takken (1970), who considered roton creation on the basis of a wave radiation model, in analogy with Cerenkov radiation. He assumed therefore that the object would, as it travelled through the superfluid, be pushing at a point of fixed phase in a roton wave pattern. He concluded that an upper bound on the velocity of a negative ion would be

you u.b.

$$v_{ub} = v_L (1 + 10^{-16} E^2), \quad (8)$$

where v_{ub} and v_L are in ms^{-1} and the electric field E is in Vm^{-1} , and therefore that, for realisable electric fields, it should be almost impossible to observe any increase in the ionic velocity beyond v_L . This remarkable conclusion appeared at the time to be in accord with Rayfield's experimental data.

Attempts by Neeper (1968) and by Neeper and Meyer (1969) to repeat Rayfield's experiments at lower temperatures, where excitation scattering could be ignored, resulted in failure. As their experimental chamber was cooled, the



vortex ring nucleation rate apparently increased until, at 0.3K, only charged vortex rings could be detected at the collecting electrode, and no bare ions. It was concluded, therefore, that neither the existence of the critical velocity predicted by Landau, nor the validity of the supercritical dissipation theory proposed by Takken, was going to be accessible to a direct experimental investigation. No reason to doubt this conclusion emerged until Phillips and McClintock (1973) observed some apparently anomalous current-pressure characteristics in a field emission cell, which they attributed to the presence of bare ions, even at temperatures as low as 0.3K.

(d) Field emission in superfluid

Field emission and field ionisation enable comparatively large currents to be injected into liquid helium, and current sources based on the phenomena have a number of advantages over the radioactive sources which were almost universally employed in the early ion experiments. If a negative potential of a few ~~µV~~ ^{kilovolts} is applied to a sharp metal tip immersed in liquid helium, then, just as in a vacuum, electrons are able to tunnel from the tip and proceed towards a collecting electrode. The presence of the liquid, however, introduces a number of complications. In particular, gaseous charge multiplication processes can take place close to the emitter; and the velocity of the ions through the liquid is drastically reduced. The latter feature of the phenomenon leads to spacecharge-limited emission at

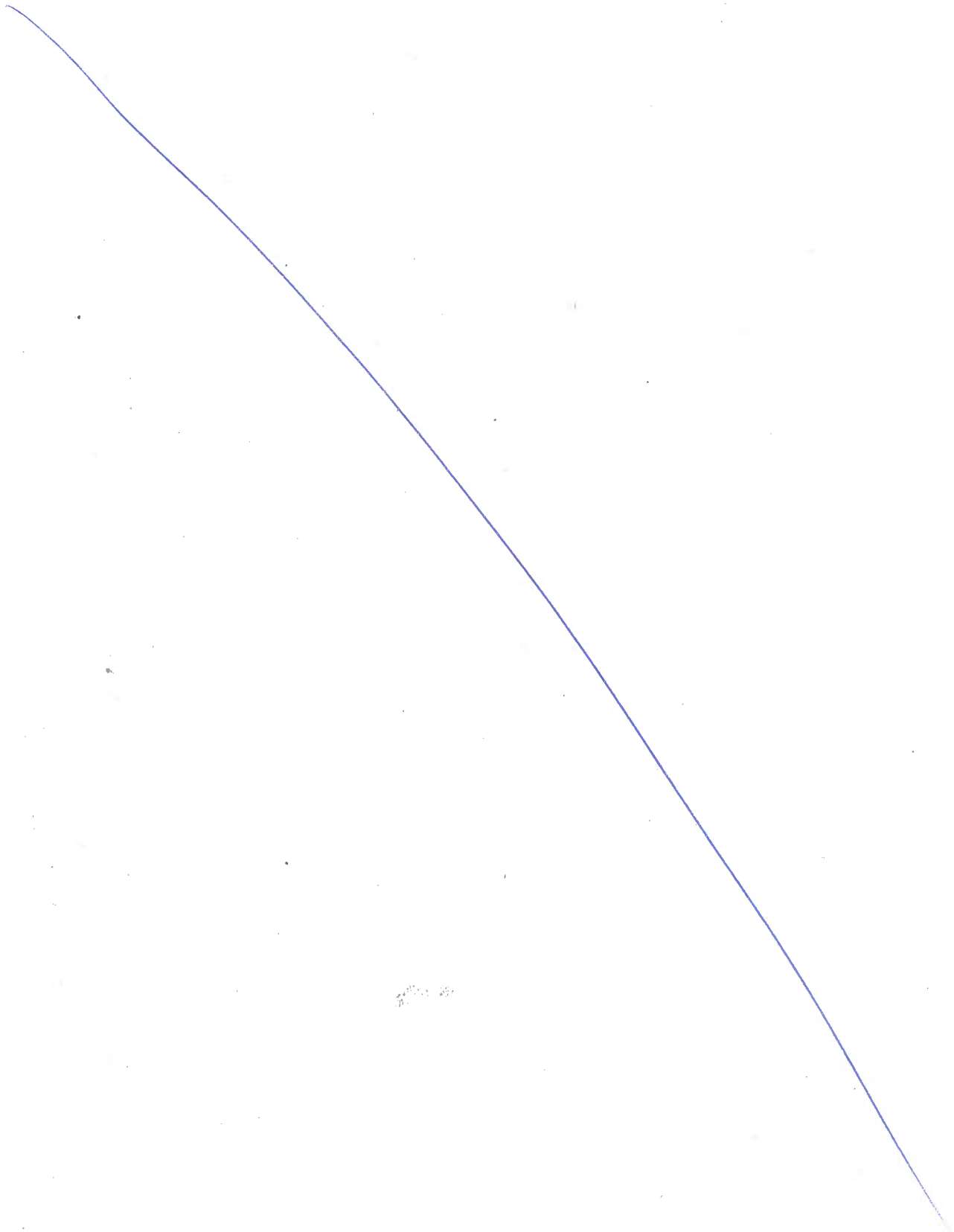
comparatively low currents $\sim 10^{-9}$ A; conversely, the magnitude of the emission current for a fixed emitter potential can provide information about the way in which the ions move through the liquid, often enabling the ionic mobility to be deduced. Field emission and ionisation in liquid ^4He have been studied in some detail by Phillips & McClintock (1975).

An observation (Phillips & McClintock (1973)) which is of special relevance to the present work relates to the field emission characteristics under pressure below 0.6K: typical examples are shown in figure 4. We note from (a) that the current rises rapidly with pressure above 10×10^5 Pa; and from (b) that the current at 25×10^5 Pa is almost temperature independent below 0.5K. These results were consistent with an increasing proportion of the current being carried by bare ions, rather than by charged vortices, as the pressure was increased beyond 10×10^5 Pa; and, furthermore, suggest that this proportion was not significantly temperature dependent near 0.3K.

The strong implication was, notwithstanding the failure of Neepers's (1968) and Neeper and Meyer's (1969) experiments, that it would, after all, probably be feasible to propagate bare ions through liquid ^4He at 0.3K at velocities up to v_L , and thus to test Landau's (1941, 1947) and Takken's (1970) theories of the breakdown of superfluidity. We describe below some of our consequent experiments in which we have succeeded in measuring the drift velocities of negative ions drawn from a field emission current source for

Figure 4
(a) and (b)

temperatures down to 0.3K. Some preliminary results of
this work (Phillips and McClintock, [#]1974; Allum, McClintock
and Phillips, ^{2H}1975a) have already been published.



2. Apparatus and Techniques

The drift velocities of the ions were measured C by using a modified form of the time-of-flight technique described by Schwarz (1972). This necessitated setting up a system capable of working under pressure, and such that suitable pulses of ions could be generated for propagation along a known length in the liquid helium. The basic technique is described in §2(a); and the experimental chamber, electrical circuitry, and cryogenic arrangements employed in its practical realization are described respectively in §2(b), (c) and (d).

(a) The single-pulse time-of-flight technique

The method is illustrated diagrammatically in figure 5. The ionic velocity is determined by measuring the transit time of a pulse of ions across a region of uniform electric field, between G_2 and G_3 , whose length is known. A retarding electric field of a few ~~kV m⁻¹~~ ^{kilovolts per metre} is usually maintained between the gate grids G_1 and G_2 , thus preventing the ions emitted from the field emission source S from entering the drift space G_2 - G_3 . By applying a negative pulse of a few tens of volts to G_1 the gate can, however, be opened momentarily, thus admitting a pulse of ions to the drift space. The ion pulse then propagates across G_2 - G_3 at a characteristic velocity which will depend on the electric field and on the temperature, pressure,

centre
fig 5
tom G



and purity of the liquid helium. Its arrival at the collecting electrode C can be observed as a pulse of current whose transit time can be used to compute the velocity. The Frisch grid G_3 is required to screen the collector from the influence of the approaching charge.

In practice we have found it necessary to pulse the field emission source, rather than running it in the d.c. emission mode and, because the resultant switching transients saturate the signal processing system, it has been necessary to delay the gate pulse relative to the start of the tip pulse as illustrated in figure 5(b). The current i_C seen at the collector is shown, in somewhat idealized form, in the lowest diagram: the transients at X and Y arise from the emitter switching on and off; and those at t_1 and t_2 are caused by the gate pulse. The rise in i_C at t_3 indicates the first appearance of ions on the collector side of G_3 , and t_4 represents their arrival at C . The passage of the back end of the pulse through G_3 occurs at t_5 , and the last ions reach the collector at t_6 . The periods $(t_4 - t_3)$ and $(t_6 - t_5)$ represent the transit time of an ion across the space between G_3 and C . The transit time τ_D between G_2 and G_3 , which we wish to measure, is $(t_5 - t_2)$.

The signal at the collector is usually comparable with, or smaller than, the intrinsic electrical noise of the system, so that some method of signal enhancement is an essential feature of the single-pulse technique. In the present work we have employed a digital signal-averaging system, as described in § 2(c) below.

(b) The experimental chamber

Figure 6

The experimental chamber is illustrated in figure 6. Its body was formed from a copper block, drilled through to accept two inserts carrying the electrode system and a carbon resistance thermometer. The inserts were built on circular brass plates which could be bolted to the block, with indium 'O' rings providing the required pressure-tight seal.

The tip, gate grids, guard rings and Frisch grid were mounted on one insert; the collector on the other. Metal components were mostly made of brass, separated by nylon spacers. Care was taken in designing the assembly, to avoid large areas of exposed dielectric on which charge might have built up, thus distorting the electric field. The grids were composed of 200 wires per inch nickel mesh, attached to brass support rings with Aquadag colloidal silver paint. It was found that, with care, a grid-to-grid spacing of 0.5 mm (measured at room temperature) was feasible. The tip itself was held approximately 2 mm away from the first grid, G_1 . At this small separation, bubble formation around the tip could have led to arcing if operated at s.v.p.: accordingly, the normal setting-up procedure entailed application of the operating pressure of 25×10^5 Pa before the emitter was tested. The whole electrode assembly was an easy sliding fit inside a nylon tube, which was itself made to be an easy sliding fit in the hole in the copper block. To promote rapid thermal equilibrium throughout

the chamber, 1 mm diameter holes were bored in the nylon sleeve, allowing good thermal contact between the copper wall of the chamber and the helium within the electrode volume.

The collector insert consisted of a brass disk surrounded by a brass guard ring, mounted on a nylon insulator. The whole was spring-mounted on its brass endplate, with a free movement of some 3 mm to ensure that during cooling and throughout the experiment the guard ring was held in firm contact with the nylon sleeve of the other insert: at room temperature the spacing between Frisch grid and collector was 0.5 mm. The same springing arrangement also served to ensure that the electrode stack in the other insert was always held under gentle compression. For both inserts, electrical connections were taken through metal-glass seals soft-soldered into the brass endplates.

The chamber dimensions were obtained by measuring the individual components at room temperature, before assembly, and then applying suitable corrections for thermal contraction. Assuming the change in length in cooling from room temperature was 2% for nylon and 0.02% for brass, the length l of the drift space (G_2 to G_3) was calculated to be 10.2 mm when cold. The possible error in this figure is thought not to exceed 5%.

(c) Electrical circuit

The circuit used to provide the required d.c. electrode

Tom CS

potentials, to apply pulses to S and G_1 , and in processing the signal arriving at C , is shown in block form in figure 7. The drift-space voltage was derived from a Keithley 246 stabilized power supply, capable of supplying 0—3100V and connected via a decoupling RC network, to a chain of 5 M Ω 1% metal film resistors. Mounted in the main liquid helium bath to reduce the number of high-tension leads into the cryostat, these resistors formed a divider network by which the tip, gate grids and guard rings could all be held at the correct d.c. potentials. This power supply was switched on only when necessary, as heating in the divider chain tended to cause a noticeably higher rate of evaporation from the helium bath. The potential difference V_D across the divider chain was measured on a Fluke 8000A digital voltmeter, floating at the G_3 potential, accurate to better than $\pm 1\%$, and supplied via a 1:1000 potential divider composed of high stability metal oxide resistors, which had been calibrated using a potentiometer. An accelerating d.c. field was established between the Frisch grid and the collector; and a retarding d.c. field was maintained between grids G_1 and G_2 to hold the gate closed. Both these fields were supplied using 90V dry cells. The d.c. bias on the gate was measured on a voltmeter floating at the gate d.c. potential. The high voltage pulses, typically 1 or 2 kilovolts, needed to cause field emission from the tungsten tip were supplied from a pulse amplifier based on the design of Robertson and Seidman (1968), driven by a Hewlett-Packard HP214A pulse

Figure 7

Tom R

Tom D



generator, and were measured on a Tektronix 453A¹⁷ oscilloscope via a Tektronix P6015 1:1000 e.h.t. probe. The pulses to open the gate were supplied from another HP214A² generator, which was also coupled to the oscilloscope via a Tektronix P601 1:10⁵ probe. The circuit's various time-constants were chosen to be such that the pulses arriving on the source and gate grid were square, and so that no pulses reached the drift space electrodes, during the flight of the ions.

The signal arriving at the collector was earthed through a 100 $\text{k}\Omega$ metal film resistor, mounted immediately next to the endplate. Screened and guarded leads connected each end of this resistor to a Brookdeal 432 High $|Z|$ differential amplifier, which had a frequency response of up to 1 MHz, mounted at the top of the cryostat. The amplified signal was stored in a Datalab DL905 transient recorder, which then passed the contents of its memory at a lower speed to a Hewlett-Packard HP5480B⁵ signal averager for processing. After averaging an appropriate number of pulses (typically 32 for the larger, high-velocity pulses, and 2048 for the smaller, low-velocity pulses), the final signal was output onto a Hewlett-Packard 7004B⁶ chart recorder, fitted with a Hewlett-Packard 17012B⁷ point plotter, to give a hard copy of the result. The transient recorder was usually kept on a slow (5 ms) scan until the tip switching transient had died away, and then switched automatically to a faster timebase (500 μs scan) for the velocity measurement itself. Typically, the gate was opened some 400 μs after

$\text{k}\Omega$

@

upright μ

the tip had been activated and was held open for 80 μs ; the ion transit time was about 200 μs , depending on the electric field; and the tip emission was maintained for about 800 μs in all. The necessary trigger delays were obtained directly from the two HP214A pulse generators. This cycle was repeated at about 3 Hz until averaging had produced a signal of acceptable quality.

(d) Cryogenics

The chamber was mounted in a ^3He cryostat of conventional design which enabled the experiment to be cooled to a working temperature of 0.28 K. The sample of ^4He was obtained from a standard high-pressure cylinder fitted with a regulator capable of delivering helium at any required pressure up to 40×10^5 Pa. The gas was cleaned by passing it over two liquid-nitrogen-temperature charcoal traps. It then passed via a 0.5 mm i.d. cupronickel capillary tube through the main liquid helium bath at 4.2 K, entered the vacuum space, and was thermally anchored to the 1.0 K pot. It there joined a 600 mm coil of 0.13 mm i.d. stainless steel capillary tube, and thence was admitted to the chamber. The pressure was measured on a Bourdon gauge (Wallace and Tieman type FA233), accurate to $\pm 0.1\%$. A three litre gas bottle was connected at the room temperature end of the system to act as a ballast volume. Using this system, pressures from 10^5 Pa up to the melting curve could be easily and fairly rapidly set, and stabilised to better than $\pm 5 \times 10^3$ Pa throughout a

sequence of measurements. When pressurizing the chamber and cooling down the cryostat, the procedures used previously (Phillips and McClintock / 1975) for the removal of air were followed, and no trouble was experienced with blockages in the capillary tubes.

The temperature T was determined by measuring the resistance of a nominal 470 Ω Speer carbon resistor, whose diameter had been reduced by grinding in order to conserve space. This thermometer was mounted inside the anode insert, in a cavity within the nylon insulator immediately behind the collector guard ring, and immersed in the sample of liquid helium. Its resistance R was measured using an a.c. bridge, and it was calibrated in the range $0.6 < T < 1.1\text{K}$ against the vapour pressure of ^3He , using an oil manometer. An empirical relationship of the form

$$\log R = A + B(\log R/T)^{1/2}$$

was employed in fitting the calibration data, using a computer programme which then prepared tables of temperature against resistance. It is estimated that the error introduced by extrapolating the relationship to 0.3K is some $\pm 20\text{mK}$ at the lowest temperatures. As will be seen in § 3, the virtual temperature invariance of the higher velocities below 0.5K made small thermometry errors relatively unimportant.

read
some ln
for log

3. Experimental Results

In this section we present a selection of our experimental measurements of the drift velocities \bar{v} of negative ions in He II, under the influence of an applied electric field E . Data is presented for $E \leq 300 \text{ kV m}^{-1}$ in the temperature and pressure ranges $0.28 \leq T \leq 0.50 \text{ K}$, $20 \leq P \leq 25 \times 10^5 \text{ Pa}$. Some representative velocity data are given in graphical form in §3(a); and a fuller set of data is tabulated in Appendix A. The dependence of signal magnitudes on electric field is described in §3(b) and the accuracy of the velocity measurements is discussed in (c). A detailed analysis of the velocity data is reserved for §4.

(a) Velocity measurements

Some typical signals recorded by the point plotter are shown in figure 8. Prior to averaging, the signals could usually not be distinguished from background noise or, as in (a), were only barely discernable. The averaging of a large number of such signals to generate a result like (b) was clearly essential for a high precision determination of the ionic velocity. Under more favourable experimental conditions, such as those of (c)-(f) where individual signals could clearly be seen, averaging was still used in order to improve the precision of the measurements. In practice, V_s was adjusted so as to avoid the pulse-spreading effects associated with signals which were too large.

Figure 8

mm 5

TAB 1

The fact that the $(t_4 : t_5)$ section of the signal is seldom flat may, at first sight, seem surprising; but there are two very simple reasons why such a phenomenon might have been anticipated. Firstly, we note that the effects of the gate-opening pulse applied to G_1 is to reduce by V_{G_1} the potential difference V_S initially applied between S and G_1 , which would certainly result in a decrease of the total emission current. Secondly, it is believed (Phillips & McClintock, 1975) that, under d.c. conditions, the spacecharge which controls the magnitude of the emission current is composed of charged vorticity, even although the bulk of the current is carried by bare ions. It will take a finite time, after activating the emitter, for the equilibrium density of charged vorticity to become established: thus, if the gate opens during this period, a decreasing current pulse will be admitted to the drift space. We believe that both these mechanisms are effective in determining the pulse-shapes which we observe in practice.

The procedure used for determining the mean velocity of the ions from an averaged pulse was to reduce it as nearly as possible to the idealised pulse shape discussed in §2(a) and illustrated in figure 5(b). From the point plotter recording of the signal, the transient point t_2 at which the gate switched off could be identified to within one channel of the 1000-channel output from the signal averager memory, resulting in a measurement error of $\pm 0.5 \mu s$. Point t_5 , where the trailing edge of the ion pulse

turn on

neu

reached the Frisch grid, was found by drawing straight lines through the top and the trailing edge of the pulse, their intersection being taken as the point t_5 . The transit time of the ions across the drift space G_2G_3 is then $\tau_D = t_5 - t_2$, and the mean velocity $\bar{v} = l/\tau_D$. The estimated error in τ_D arising from this procedure is $\pm 0.5\%$ of the transient time. For the larger, better defined, pulses the total error in τ_D is estimated as less than 1%; and as less than 2% for all the data presented in Appendix A.

We note that the leading edge of the pulse (t_3 to t_4) traverses the gate region of the chamber, while the trailing edge does not. Thus any complications which occur inside the gate may affect the apparent transit time as determined from leading edge instruments, but not that obtained using the trailing edge. For this reason the trailing edge has been used throughout in order to determine the transit time of the pulse.

Schwarz (1972) has pointed out that the signal received at the collector is modified by the detecting electronics due to their finite rise time, and that points on the pulse found by the method described above should be corrected by subtracting a time $0.25\tau_e$ where τ_e is the rise time of the detector. The rise time of the circuit used in the present work was $\approx 2\mu s$ and, as the typical ion transit time was $\approx 200\mu s$, such a correction would have had a negligible effect, and has therefore not been applied.

↑
m e



Some typical $\bar{v}(E)$ experimental data are shown in figure 9. Results at 0.29K for two pressures are shown in (a). At the lower pressure it was found impossible to detect the arrival of bare ions below $E \approx 120 \text{ kV m}^{-1}$ although at $25 \times 10^5 \text{ Pa}$ pulses were sometimes clearly visible down to $\approx 1 \text{ kV m}^{-1}$. We discuss this point in more detail in § 3(b) below.

The influence of the temperature on the $\bar{v}(E)$ characteristic is shown in figure 9(b). As T is raised the change at low E becomes evident, with a much more rapid dependence of \bar{v} on E than at higher fields. This may be attributed to the increasing importance of phonon scattering as T is increased. Above $\approx 60 \text{ kV m}^{-1}$, the measured drift velocities were found to be independent of T , within the experimental error, for $T \leq 0.5\text{K}$. A fuller set of velocity data is tabulated in Appendix A.

(b) Signal magnitudes

The magnitude i_c of the received signal was found to vary in a complicated manner with E , P and T , even although all other experimental parameters were kept constant. The circuit (figure 7) was designed in such a way that E could be varied over a wide range without affecting in any way the potential differences between other parts of the electrode system. In practice, with P and T held constant, it was found that i_c , taken as the height of the signal at t_5 (figure 4(b)), varied rapidly with E , typical results being shown in figure 10. It was difficult to obtain reliable values of i_c , as a function of E , for pressures

Figure 9
(a) and (b)

from c

Figure 10
(a) and (b)



much below 25×10^5 Pa. The reason was that, in order to obtain a signal of a measurable size, it was necessary to increase the magnitude of the tip pulse V_s (figure 5), causing a small but significant degradation of the emission tip with time and resulting in apparent hysteresis effects in the $i_c(E)$ data. At 25×10^5 Pa, however, a relatively low value of V_s could be used to provide reproducible results, such as those of figure 10, on any given occasion (although an apparent dependence on the sample of ^4He was observed: see below).

Because, in plots such as figure 10, E was the only parameter being varied and the grids, under our experimental conditions, could be regarded as retaining their geometrical transparency, this behaviour must be attributed to field dependent events inside the drift region itself. The most probable explanation would seem to lie in a field dependence of the vortex ring nucleation rate ν : any ion creating a (relatively very slow) charged vortex ring will, effectively, be completely lost from the bare ion pulse. Acting on this assumption it is possible (Phillips and McClintock, 1975) to deduce values of ν from the data.

A number of aspects of the phenomenon are, however, still rather mysterious. In particular, we have found that the magnitude of the signals tends rapidly to get smaller as T is reduced, whereas figure 4(b) strongly suggests that the current from the tip is temperature independent below 0.5K . Furthermore, figure 4(a) appears to imply that we

should be able to observe strong bare ion signals down at least to a pressure of 15×10^5 Pa, and perhaps below, whereas we have in practice been quite unable to observe signals for pressures lower than 20×10^5 Pa.

Certain features of the data have also seemed to be irreproducible between experimental runs, notably the value of E below which the bare ion signal disappears for $T = 0.3$ K: in our preliminary experiments (Phillips and McClintock, 1974) no signals could be detected below 60 kV m^{-1} whereas, subsequently (Allum, McClintock and Phillips, 1975a), it proved possible to follow the signal down to 2 kV m^{-1} . The only obvious difference between the two experiments seemed to be that the main ^4He cylinder had been refilled in the interim, thus raising the possibility that small differences in the isotopic impurity level might have occurred, and might be important. Very recent experiments (Allum and McClintock, to be published), in which minute quantities of ^3He have been added to the sample of ^4He , have apparently confirmed this hypothesis: the presence of 1 p.p.m. of ^3He is sufficient to prevent any bare ion signals at all being observed below about 0.5 K. An explanation of these results can be devised on the assumption that ^3He atoms condense on the negative ions (Dahm, 1969) and on the vortex lines and rings (Ostermeier, Yarmchuk and Glaberson, 1975) which will be formed throughout the chamber; but the situation is clearly very complicated, deserves further investigation, and will be discussed in more detail elsewhere.

(c) Accuracy

The main source of error in \bar{v} arises from the uncertainty in the length of the drift space l which, as discussed in § 2(b), is believed to be less than $\pm 5\%$. However, by comparing ionic mobilities $\mu (= \bar{v}/E)$ measured at low fields for temperatures μ/k , with the higher precision measurements of other workers (who used longer drift spaces), this uncertainty can be reduced somewhat. A satisfactory comparison with Ostermeier's (1973) mobilities is not feasible because the overlap of experimental ranges occurs in the region where it is now known that 'anomalous' curvature exists in the $\bar{v}(E)$ characteristic (Allum, McClintock & Phillips 1975b; Bowley 1976). Thus our data, which could only be obtained for $E > 1/kV/m^{-1}$, are not strictly comparable with those of Ostermeier for $E < 0.1 kV/m^{-1}$. Brody (1975), however, has measured μ in fields of typically $10 kV/m^{-1}$ and comparison of our data with his yields good agreement. Taking account of errors in both sets of measurements we conclude that the uncertainty in the length of our drift space is $\pm 3\%$ and thus that $l = 10.2 \pm 0.3$ mm.

Investigations were made of the effect on the received signals of alterations in the gate pulse length and magnitude; the tip pulse length and magnitude; and their relative positions in time. Although some slight variations in signal pulse shape were found, the drift velocities \bar{v} remained constant within the experimental error. No effects attributable to heating of the sample by the ion current

were observed.

Random errors in \bar{v} arising from residual noise on the averaged pulses, and from the technique used in obtaining v from the point plotter recordings, show up as scatter in the results, typically $\pm 0.5 \text{ ms}^{-1}$ or less for the higher fields and pressures and about $\pm 1 \text{ ms}^{-1}$ where experimental conditions are less favourable.

We conclude, therefore, that the data tabulated in Appendix A are subject to a common systematic uncertainty of $\pm 3\%$ in their absolute values; and that, in addition, there is a random error whose magnitude can be estimated from the scatter of a particular set of data points about a smooth curve, but which is usually in the region of 1 - 2%. The possible systematic error of $\pm 2\%$ in V_D means that there will be an error in E of up to $\pm 5\%$.

4. Discussion

In this section we discuss our experimental data in the light of various theoretical predictions as to the form of $\bar{v}(E)$. We compare our data with Landau's theory of superfluidity in (a). In (b) we suggest some reasons why our data are inconsistent with Takken's (1970) supercritical drag theory, and in (c) we discuss how supercritical energy dissipation by a light moving object may be expected to differ from that caused by a very heavy object. We review Bowley & Sheard's (1975) calculations of supercritical drag through single-roton and two-roton emission processes, and compare our data with their theories, in (d) and (e) respectively. Finally, in (f), we include a brief speculative discussion of our apparent failure to find any evidence of the occurrence of one-roton processes.

(a) Comparison with Landau's theory

We note from figure 9 that our $\bar{v}(E)$ data appear to be very much what would be expected on the basis of Landau's theory. This becomes more immediately evident when we plot the net drag on the ion ($=eE$) as a function of its average velocity through the superfluid, as shown in figure 11: the result at 0.35K can then be seen to bear a close resemblance to the behaviour depicted in figure 3 and, moreover, the critical velocity which we observe appears to be equal to v_L within experimental error. For comparison, the corresponding curve for a negative ion in

Figure 11



normal (non-superfluid) liquid ^4He , where it can be characterised by a constant mobility, has also been plotted. The behaviour is seen to be qualitatively different in the two cases.

The pressure dependence of the critical velocity is also of interest. Because a decrease in pressure results in an increase in Δ and a decrease in k_0 , we expect that $v_L \approx \Delta/k_0$ will increase as the pressure is reduced below 25×10^5 Pa. It may be seen from figure 9(a) that, although data at 21×10^5 Pa could not be obtained for low electric fields, the 21×10^5 Pa $\bar{v}(E)$ curve lies above that for 25×10^5 Pa which seems to imply a change of v_L with P in the expected direction. We will return to discuss this point in more detail, on the basis of Bowley and Sheard's (1975) theory of supercritical drag, in §11(e).

We conclude that our experimental data amount to a striking verification of Landau's (1941, 1947) explanation of superfluidity in liquid ^4He .

(b) The failure of Takken's theory

As discussed in §1(c) above, Takken's (1970) theory predicted that it should be almost impossible experimentally to cause ions to exceed v_L to a measurable extent. On the basis of (8) we would expect \bar{v} to exceed v_L by less than $4 \times 10^{-4}\%$ when $E = 200 \text{ kVm}^{-1}$ whereas it can be seen in figure 9 that the margin is, in reality, about 18%. Furthermore, the form of the observed $\bar{v}(E)$ curve is quite different to that predicted by (8), which would bend upwards on plots such as those of figure 9. It seems clear, therefore, that

Takken's theory is not applicable to the motion of negative ions through pressurised He II below 0.5K . The reason is probably connected with the relatively small mass of the ion.

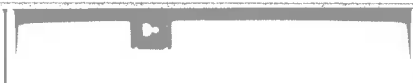
The assumption that roton creation is a coherent process is of doubtful validity unless the mass of the moving object is very large. There are two reasons for this. Firstly, the object will have a random thermal velocity of $v_t \approx (3k_B T/m)^{1/2}$; and, secondly, conservation of momentum dictates that, in emitting a roton, the forward momentum of the object be reduced by an amount $\Delta v_1 \approx \hbar k_0/m$. Unless m is very large, each of these effects will have a tendency to destroy any incipient phase coherence between the roton creation events. As discussed in § 4(c) below, the mass of the negative ion in the He II under 25×10^5 Pa pressure is probably about $72m_4$ where m_4 is the ^4He atomic mass, leading to $v_t \approx 5\text{ms}^{-1}$ and $\Delta v_1 \approx 5\text{ms}^{-1}$. Under our experimental conditions, therefore, v_t and Δv_1 each amount to about 10% of the average total velocity of the ion so that, in retrospect at least, it is not at all surprising that Takken's theory does not seem able to describe the physical situation which we have been investigating.

We require a new theory which makes no assumption of phase coherence, and which takes explicit account of the recoil of the ion every time it emits a roton.

(c) Critical energy dissipation by a light object

In the case of a light object, the second term in (3) cannot be ignored, and the critical initial velocity v_1' for the emission of a roton may become substantially greater

Q
upright



than v_L . The ionic velocity \bar{v} which we measure experimentally is, however, a time-averaged value over many roton creation events: we shall see that \bar{v} need not be significantly larger than v_L , even though v_1' may be. As will be discussed in more detail in § 4(d), we will assume that the influence on \bar{v} of the fluctuating thermal velocity of the ion can, to a good approximation, be ignored.

We consider first an object travelling through superfluid ^4He at a very low temperature such that the drag arising from the scattering of thermal excitations can be neglected, and under the influence of a force which is sufficiently weak that roton emission will occur at a velocity negligibly larger than v_1' . Under these conditions the angle θ between the direction in which the object is travelling and that in which the momentum of the roton is directed, is zero, and the problem is one-dimensional. We assume that the emitted roton has energy ϵ_1' , momentum $\hbar k_1'$, and that the final velocity of the object, after emission is v_1'' . Then (3) becomes

$$v_1' = \left(\frac{\epsilon_1'}{\hbar k_1'} + \hbar k_1' / 2m \right) \quad (9)$$

In order to conserve momentum

$$mv_1' = mv_1'' + \hbar k_1'$$

so that

$$v_1'' = v_1' - \hbar k_1' / m$$

which, using (9) becomes

$$v_1'' = \frac{\epsilon_1'}{\hbar k_1'} - \hbar k_1' / 2m \quad (10)$$

primes v_1'



ten

From (9) and (10), the average velocity for the onset of dissipation which we measure experimentally,

$$\bar{v}_{c1} = \frac{1}{2}(v_1' + v_1'') = \epsilon_1' / \hbar k_1' \quad (11)$$

and the instantaneous velocity of the object as a function of time must be as depicted in figure 12(a). To compute numerical values of v_1' , v_1'' and \bar{v}_{c1} for an object of any given mass we need to find the value of k which makes the right hand side of (3) a minimum. Differentiating it with respect to k , and setting equal to zero to find k' ,

$$\frac{1}{\hbar} \left(\frac{d\epsilon}{dk} \right)_{k_1'} = \frac{\epsilon_1'}{\hbar k_1'} - \frac{\hbar k_1'}{2m} \quad (12)$$

which, using (5) to substitute for ϵ_1' , becomes

$$\frac{\hbar(k_1' - k_0)}{m} = \frac{\Delta}{\hbar k_1'} + \frac{\hbar^2 (k_1' - k_0)^2}{2m \hbar k_1'} - \frac{\hbar k_1'}{2m} \quad (13)$$

We have solved this equation numerically for k_1' , using various values of m and assuming Donnelly's (1972) roton parameters at 25×10^5 Pa and have then used (5), (9) and (11) to find v_1' , \bar{v}_{c1} and v_1'' . The results are displayed in figure 13. It is clear that although the recoil of the object, as indicated by the difference between v_1' and v_1'' , is significant even for effective masses as large as a few hundred times m_4 , the critical time-averaged velocity \bar{v}_{c1} hardly deviates from v_L provided that $m > 30m_4$.

It is interesting to note that for very light objects ($m < 3.5m_4$) v_1'' becomes negative, implying that the ion will be moving backwards immediately after emitting the roton. So, also, will be the roton because, comparing (10) and (12),

fig 12

13

fig 13



new

we can see that v_1'' is numerically equal to the roton's group velocity. Thus a bizarre situation can arise whereby an ion which is initially moving forwards can dissipate some of its kinetic energy by creating a roton moving backwards, and yet conserve energy and momentum in the process, despite the fact that its own final velocity will also be in the backwards direction. The roton's momentum, however, being related to its phase velocity which by (11) is numerically equal to the time-averaged velocity $\bar{v}_{(c1)}$ of the object, remains positive.

The negative ion, which may be regarded as a non-localized electron trapped within a spherical void in the liquid, has an effective mass which is almost entirely hydrodynamic in nature and which therefore depends only on the ionic radius r_i and the density ρ of the liquid. The effective mass has been determined directly only under the saturated vapour pressure: Poitrenaud and Williams (1972, 1974) were able to observe the resonance of ions trapped in the potential well just beneath the free liquid surface, from which they concluded that $m_i = (243 \pm 5)m_4$. This value is consistent with the hydrodynamic mass $(= 2 \pi \rho r_i^3/3)$ which may be deduced from values of the ionic radius measured by other means. Information concerning ionic radii at different pressures has been derived from a number of sources including, particularly, measurements of the mobility and of the trapping lifetime on superfluid vortices; and the data are found to be in satisfactory agreement with the simple bubble model first described by Kuper (1961) and subsequently developed by Springett, Cohen and Jortner (1967).

upright pi



The available experimental information has been correlated, on the basis of this model, by Schwarz (1975) who has concluded that the ionic radius at 25×10^5 Pa is between 1.08 and 1.12[#]nm, depending on the precise value taken for the surface tension under pressure. Assuming a liquid density of 172 kg m^{-3} , the corresponding hydrodynamic mass lies between 68 and $76m_4$: we shall therefore assume a value of $72m_4$.

From figure 13 it can be seen that, for an ion of this mass, although $(v_1' - v_1'')$ is about 10% of \bar{v}_{c1} , $\bar{v}_{c1} \approx v_L$ to an excellent approximation, and we may therefore write (9)-(11) in the forms

$$v_1' = v_L + \hbar k_o / 2m_i \quad (14)$$

$$v_1'' = v_L - \hbar k_o / 2m_i \quad (15)$$

and

$$\bar{v}_{c1} = v_L \quad (16)$$

with negligible error. Thus, although by (14) the ion has to reach a critical instantaneous velocity v_1' for single-roton creation which is 2.5 ms^{-1} larger than the Landau critical velocity v_L appropriate to an object of infinite mass, the drift velocity \bar{v} at which dissipation is observed to commence experimentally should nevertheless be very closely equal to v_L .

(d) Supercritical energy dissipation: single-roton emission

We find experimentally that quite modest electric fields are sufficient to propel the ions at drift velocities which are several ms^{-1} ^{metres per second} larger than v_L . Since $\epsilon_1' / \hbar k_1'$ is closely equal to v_L we conclude that, if the dissipative process involves the emission of single rotons, then the instantaneous velocity as a function of time must be something like the graph sketched in figure 14: the ion must, on average,

Figure 14



continue to accelerate for a finite time τ_1 after the conservation laws for roton emission can be satisfied, before the roton is emitted: on average, it is travelling at a velocity v_{e1} ($> v_1'$) immediately before emitting the roton, and at a velocity v_{f1} immediately afterwards, having had its velocity reduced by $\Delta v_1 = v_{e1} - v_{f1}$. A convenient way of approaching the problem theoretically is to postulate that there exists a matrix element which determines the strength of the roton emission process, and then to calculate the form of $\bar{v}(E)$ which would then be expected, leaving the matrix element as an unknown constant to be determined by experiment. This procedure has been carried out by Bowley & Sheard (1975) and we outline below, in a somewhat simplified form, the salient features of their calculation.

Before we do so, however, it is necessary to consider in more detail the influence of the dilute excitation gas, consisting mainly of phonons and ^3He isotopic impurities but also including a few rotons, through which the ion is moving. At low temperatures in pure ^4He , roton emission will tend to be the principal mechanism limiting the drift velocity of the ion, but there will of course also be a contribution to the net drag on the ion arising from the scattering of excitations. Furthermore, because of the relatively small ionic mass, individual scattering events will cause significant changes in the instantaneous velocity of the ion. To look at the situation in another way, the ion will tend to have a superimposed random thermal velocity amounting to about 8% of its average velocity in the direction of the electric field. Roton emission occurs, however, with a frequency



zero \uparrow
of about eE/k_0 , this being the inverse of the time taken by the ion to increase its velocity by k_0/m_i . Except for very small values of E, this frequency is much larger than the rate of excitation scattering events, and we may therefore conclude that the influence on \bar{v} of thermal fluctuations in the ionic velocity parallel to the field may be ignored.

The effect on \bar{v} of thermal velocity fluctuations perpendicular to the field is more subtle. The quantity which we measure experimentally is the time-averaged velocity component parallel to the field; but the time-averaged total velocity will be larger because of the transverse thermal velocity of $\approx 4 \text{ m s}^{-1}$. The measured value of $\bar{v} \approx 50 \text{ m s}^{-1}$ will thus be smaller by about 0.4% than the average total velocity, which implies that the Landau critical velocity as deduced from the data will be smaller by about 0.2 m s^{-1} than its true value. The magnitude of the difference will, of course, be temperature dependent, so we may anticipate that the apparent value of v_L will increase as the temperature is reduced. These effects will, however, be smaller than other uncertainties in our measurements.

We conclude that, for the range of electric fields and temperatures used in the present experiment, the net effect on \bar{v} of thermal fluctuations in the ionic velocity is, to a good approximation, zero.

For an ion travelling precisely at v' there is only one state into which a roton can be emitted, while satisfying the conservation laws, and so the transition rate is negligibly small. As the ion accelerates beyond v' , however, the rate $R_1(v)$ rises rapidly because of the increase in the number of possible final roton states.

As suggested by Reif and Meyer (1960), it is convenient to treat this problem using Fermi's golden rule

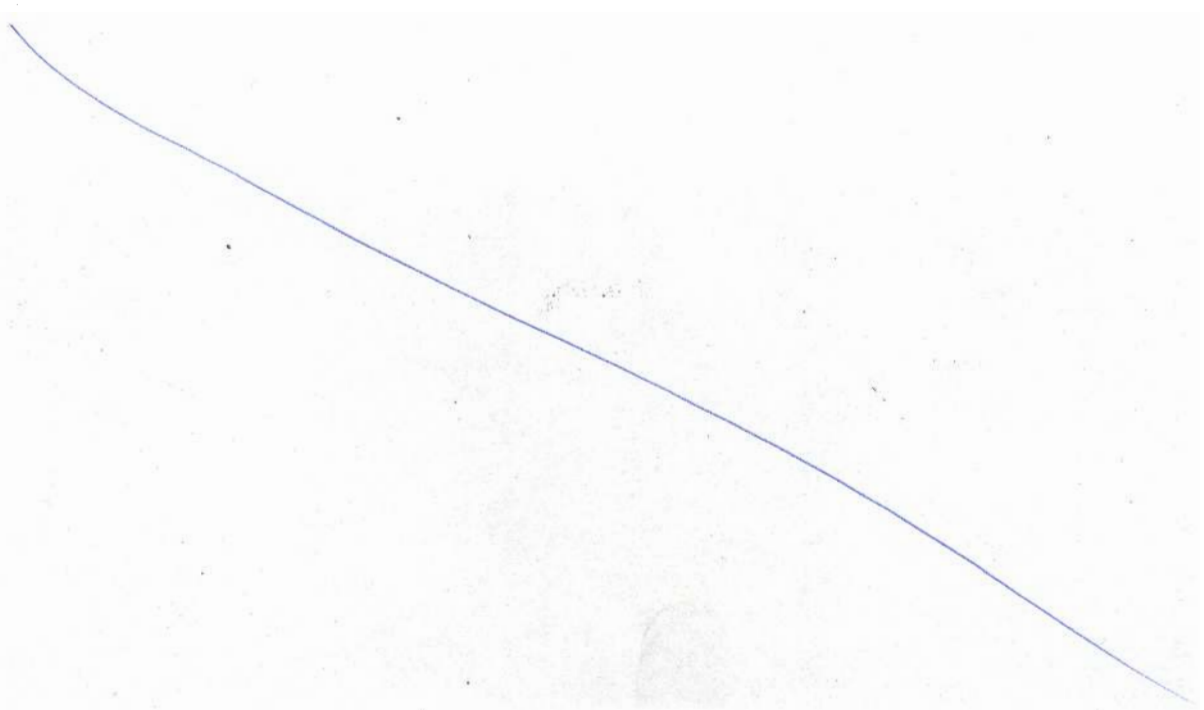
upright pi pi, Σ
 - hold stat

$$R_1(v) = \frac{2\pi}{\hbar} \sum_{\underline{k}} |V_{\underline{k}}|^2 \delta\left(\epsilon + \frac{\hbar^2 k^2}{2m_i} - \hbar \underline{k} \cdot \underline{v}\right) \quad (17)$$

trans on st
 mid pt

where $V_{\underline{k}}$ is the unknown matrix element, ϵ and $\hbar \underline{k}$ the energy and momentum of the emitted roton, m_i is the mass of the ion and \underline{v} its velocity immediately prior to emission, and the δ -function ensures conservation of energy. Evaluating

rom i



the sum over all possible final states and assuming V_k ^B is constant ($=V_{k_0}$) over the range of interest (Appendix ^I ~~II~~), we obtain

$$R_1(v) = \alpha (v - v_1')^{1/2}, \quad (18)$$

where

$$\alpha = \frac{|V_{k_0}|^2 (2m_e)^{1/2} k_0^{-3/2}}{\pi \hbar^{5/2} v} \quad (19)$$

Although v appears in the denominator of the expression for α , we assume that its variation with E is so very much slower than that of $(v - v_1')$, that we may regard α as being constant within the velocity range of interest. We will also assume that the momentum lost by the ion in creating a roton is always $\hbar k_0$: in fact, of course, there will be a spread of momenta centred approximately on k_0 ; but the shape of the dispersion curve implies that, within the momentum range of interest, this spread is always small compared with k_0 . Thus, in a plot such as that of figure 14, we assume that the effect of increasing E is to raise the sawtooth waveform to higher velocities and to reduce its period, but without causing any significant change in its amplitude: the velocity lost by the ion as a result of emission, to a very good approximation, is

$$\Delta v_1 = \hbar k_0 / m_i \quad (20)$$

We will define the average time τ_1 which elapses with $v > v_1'$ before roton creation occurs as

$$\int_0^{\tau_1} R_1(v) dt = 1 \quad (21)$$

Assuming that $t = 0$ at $v = v_1'$, which can usually be true provided that $v_{(f)} < v_1'$ (a condition which, in terms of measurable variables, implies $\bar{v}_1 < v_L + \Delta v_1$, where \bar{v}_1 is the drift velocity of the ion when limited by single-roton emission events),

$$v = v_1' + \left(\frac{eE}{m_i}\right) t. \quad (22)$$

If we use

using (18) to substitute for $R_1(v)$, and (22) for v , (21) becomes

$$\int_0^{\tau_1} \alpha \left(\frac{eE}{m_i}\right)^{1/2} t^{1/2} dt = 1, \quad (23)$$

whence

$$\tau_1 = \left(\frac{3}{2\alpha}\right)^{2/3} \left(\frac{m_i}{eE}\right)^{1/3}. \quad (24)$$

From figure 14 it is clear that

$$\bar{v}_1 = v_L + \left(\frac{eE}{m_i}\right) \tau_1, \quad (25)$$

so that we obtain

$$\bar{v}_1 = v_L + \left(\frac{3e}{2\alpha m}\right)^{2/3} E^{2/3}. \quad (26)$$

We still need to consider the high velocity situation where $v_{(f)} > v_1'$. In this case $t = 0$ at $v = v_{(f)}$ and instead of (22) we obtain

$$v = v_{(f)} + \left(\frac{eE}{m_i}\right) t. \quad (27)$$

Inserting this, with (18), into (20) we find

$$\int_0^{\tau_1} \alpha \left(v_{(f)} + \left(\frac{eE}{m_i}\right) t - v_1'\right)^{1/2} dt = 1, \quad (28)$$

which yields

$$(v_{f1} + \frac{eE}{m_i} \tau_1 - v_1')^{3/2} - (v_{f1} - v_1')^{3/2} = \frac{3eE}{2m_i \alpha} \quad (29)$$

Now, from figure 14(b),

$$\bar{v}_1 - v_L = v_{f1} + eE\tau_1 / m_i - v_1' \quad (30)$$

so that (28) becomes

$$(\bar{v}_1 - v_L)^{3/2} - (\bar{v}_1 - v_L - \Delta v_1)^{3/2} = \frac{3eE}{2m_i \alpha} \quad (31)$$

where we have also noted that $eE\tau_1 / m_i = \Delta v_1$.

Finally, we observe that (26) and (31) can conveniently be combined to give an equation which holds true for $\bar{v}_1(E)$ both above and below v_1' :

$$(\bar{v}_1 - v_L)^{3/2} - (\bar{v}_1 - v_L - \Delta v_1)^{3/2} \theta(\bar{v}_1 - v_L - \Delta v_1) = \frac{3eE}{2m_i \alpha} \quad (32)$$

where θ is the unit step function. By solving this equation we can determine $\bar{v}_1(E)$, appropriate to energy dissipation through single-roton emission processes, over a wide range of E , for comparison with our experimental results.

We note that a more rigorous theoretical analysis by Bowley & Sheard (1975) in which they have eschewed the concept of an average pre-emission time τ_1 but, instead, have set up and solved the appropriate Boltzmann equation, results merely in an additional factor of

$$\int_0^\infty (\exp(-y^{3/2}) dy = 0.903$$

multiplying the right hand side of (32).

Before comparing the equation with our data, it is of interest to consider its limiting behaviour. For $\bar{v}_1 < v_L + \Delta v_1$

upright 



one naturally re-obtains (26). For \bar{v}_1 slightly greater than $v_L + \Delta v_1$ there is, of course, no simple analytic form of $\bar{v}_1(E)$. For $\bar{v}_1 - v_L \gg \Delta v_1$, however, which is equivalent to the assumption of $m \rightarrow \infty$ so that Δv_1 then becomes negligible, we can usefully expand $(\bar{v}_1 - v_L - \Delta v_1)^{3/2}$ using the binominal theorem, whereby (32) becomes

$$(\bar{v}_1 - v_L)^{3/2} = (\bar{v}_1 - v_L)^{3/2} \left[1 - \frac{\Delta v_1}{2(\bar{v}_1 - v_L)} + \dots \right] = \frac{3eE}{2m_1 \alpha}$$

or, using (20),

$$\bar{v}_1 \approx v_L + \left(\frac{e}{\alpha \hbar k_0} \right)^2 E^2 \quad (33)$$

independent of mass and

which is of the same form as the expression (8) which Takken (1970) derived using the implicit assumption of a very heavy ion.

If we assume, that $m_1 = 72m_4$,

then we find $\Delta v_1 = 4.5 \frac{m_4}{m_1} \text{ms}^{-1}$. Thus, for $\bar{v}_1 < 5 \frac{m_4}{m_1} \text{ms}^{-1}$, (26) should be applicable and we would therefore expect a plot of \bar{v} against $E^{2/3}$ to yield a straight line which would be extrapolated back to v_L ; while, for higher velocities, we would anticipate deviations such that $\frac{d^2 \bar{v}}{d(E^{2/3})^2}$ becomes positive and the data fall above the line. In figure 15 we show such a comparison with (26) : it is quite impossible to draw a plausible straight line through any portion of the data and, furthermore, $\frac{d^2 \bar{v}}{d(E^{2/3})^2}$ remains negative throughout the whole experimental range of \bar{v} .

It is clear that (32) is unable to describe the experimentally observed form of $\bar{v}(E)$ and we conclude, therefore, that the ions do not dissipate the energy acquired from the electric field through creation of single rotons.

Figure 15



(e) Supercritical energy dissipation: two-roton emission

If we suppose that, for some unknown reason, the ion cannot emit a single roton, then it will continue to accelerate, eventually reaching the critical velocity v_2' necessary for the simultaneous emission of two rotons. Following arguments similar to those used in deriving (3), and assuming that both rotons have the same wave vector, we find

$$v_2' = (\epsilon/\hbar k + \hbar k/m)_{\min} \quad (34)$$

Assuming that k_2' is the value of k which minimizes the right hand side of (34), we can use conservation of momentum to show that if emission takes place at the critical velocity, the velocities of the ion immediately before and after are

$$v_2^{\prime} = \epsilon_2' / \hbar k_2' + \hbar k_2' / m_i \quad (35)$$

and

$$v_2'' = \epsilon_2' / \hbar k_2' - \hbar k_2' / m_i \quad (36)$$

so that the average ionic velocity,

$$\bar{v}_{c2} = \epsilon' / \hbar k_2' \quad (37)$$

for critical dissipation.

To compute numerical values of \bar{v}_{c2} , v_2' and v_2'' we follow a similar procedure to that used above for single roton emission. The equation, analogous to (13), which determines k' is

$$\hbar(k_2' - k_0) / m_i = \Delta / \hbar k_2' + \hbar(k_2' - k_0)^2 / 2m_r k' - \hbar k_2' / m_i \quad (38)$$

numerical solutions of which have been used in calculating



the values of \bar{v}_{c2} , v_2' and \bar{v}_2'' displayed in figure 13. We see that, for an ion of mass about $72m_4$, it is an excellent approximation, as in the case of single-roton emission, to assume that $\bar{v}_{c2} = v_L$; and thus that, in (35) and (36), we can replace the ϵ_2' and k_2' by Δ and k_0 respectively. Hence, in analogy to (14-16) for single-roton emission, we now obtain

$$v_2' = v_L + \hbar k_0 / m_i \quad (39)$$

$$v_2'' = v_L - \hbar k_0 / m_i \quad (40)$$

and $\bar{v}_{c2} = v_L \quad (41)$

The $v(t)$ behaviour of an ion which dissipates energy through two-roton emission should therefore be as depicted in figure 12(b): for any given electric field, the amplitude and period of the sawtooth will be twice as large as those in the single-roton case.

Figure 16

We treat two-roton supercritical dissipation by employing a similar approach (figure 16) to that used for the single-roton emission case in § 4(c), above. Again, following Bowley and Sheard (1975), we can write down an expression for the emission rate

$$R_2(v) = \frac{2\pi}{\hbar} \sum_k \sum_q \frac{|V_{kq}|^2}{\Omega^2} \delta \left\{ \epsilon_k + \epsilon_q - \hbar(k+q) \cdot v + \frac{\hbar^2(k+q)^2}{2m_i} \right\} \quad (42)$$

mid pt

Here, $V_{k,q}$ is the unknown matrix element which permits the ion to create a pair of rotons with momenta $\hbar k$ and $\hbar q$, and the other symbols have the same significance as before.



Summing over all possible final roton states it can be shown (Appendix ~~IV~~^C) that

$$R_2(v) = \beta (v - v_2')^2 \quad (43)$$

where

$$\beta = \frac{k_0^4 |V_{k_0, k_0}|^2 m_0}{2\pi^2 h^3 v^2} \quad (44)$$

and, again, we suppose that v^2 varies so much more slowly than $(v - v_2')^2$ that we can regard β as remaining constant within the velocity range of interest. The average increment of ionic velocity $\Delta v_2 = v_{e2} - v_{i2}$ lost as a result of each emission event will be twice as large as before, so that

$$\Delta v_2 = \frac{2\hbar k_0}{m_i} \quad (45)$$

assuming once more that all the emitted rotons have momenta approximately equal to $\hbar k_0$.

We define the average time τ_2 which elapses with $v > v_2'$ before emission occurs by

$$\int_0^{\tau_2} R_2(v) dt = 1 \quad (46)$$

Provided that $v_{e2} < v_2'$ (i.e. $\bar{v}_2 < v_L + \Delta v_2$),

$$v = v_2' + (eE/m_i) t \quad (47)$$

and so, ^{by} using (43), (46) becomes

$$\int_0^{\tau_2} \beta (eE/m_i)^2 t^2 dt = 1 \quad (48)$$

whence

$$\tau_2 = (3/\beta)^{1/3} (m_i/eE)^{2/3} . \quad (49)$$

It is clear (figure 16(a)) that

$$\bar{v}_2 = v_L + (eE/m_i) \tau_2 , \quad (50)$$

which, using (49), becomes

$$\bar{v}_2 = v_L + (3e/\beta m_i)^{1/3} E^{1/3} . \quad (51)$$

It is interesting to note that this is similar in form to the analogous equation (26) for single-roton emission, except that the $\frac{2}{3}$ power law has now been replaced by a $\frac{1}{3}$ law.

We must also consider the case of $v_{f2} > v_2'$, for which (47) is replaced by

$$v = v_{f2} + (eE/m_i) t . \quad (52)$$

Thus instead of (48) we obtain

$$\int_0^{\tau_2} \beta [v_{f2} + (eE/m_i) t - v_2']^2 dt = 1 , \quad (53)$$

yielding

$$(v_{f2} + eE\tau_2/m_i - v_2')^3 - (v_{f2} - v_2')^3 = 3eE/\beta m_i \quad (54)$$

Now (figure 16(b))

$$\bar{v}_2 - v_L = v_{f2} + (eE\tau_2/m_i) - v_2' , \quad (55)$$

so (54) becomes

$$(\bar{v}_2 - v_L)^3 - (\bar{v}_2 - v_L - v_2)^3 = 3eE/\beta m_i , \quad (56)$$

where we have also noted that $eE\tau_2/m_i = 2\hbar k_0/m_i$, and used (45). This equation can be solved for \bar{v}_2 but, first,

it is convenient to combine it with (51) to give a general expression which holds true for \bar{v}_2 both above and below

$$v_L + \Delta v_2: \quad (\bar{v}_2 - v_L)^3 - (\bar{v}_2 - v_L - \Delta v_2)^3 \theta (\bar{v}_2 - v_L - \Delta v_2) = 3eE/\beta m_L \quad (57)$$

This equation, which is analogous to (32) for the single-roton case, describes $\bar{v}_2(E)$ for dissipation through two-roton emission processes over a wide range of E. Again, Bowley and Sheard (1975) have shown that a more rigorous theoretical analysis, based on the solution of a Boltzmann equation rather than relying on the concept of an average pre-emission period τ_2 , results only in a small numerical modification of the equation. In this case, the right hand side of (57) should be multiplied by $\int_0^\infty e^{-y^3} dy = 0.893$ to obtain a more exact version of the equation.

Returning now to (56) we obtain, after a little manipulation,

$$(\bar{v}_2 - v_L)^2 - \Delta v_2 (\bar{v}_2 - v_L) + \frac{1}{3} \Delta v_2^2 - eE/\beta m_L \Delta v_2 = 0,$$

which is quadratic in $(\bar{v}_2 - v_L)$. Solving this,

$$\bar{v}_2 = v_L + \frac{1}{2} \Delta v_2 \left[1 + (4eE/\beta m_L \Delta v_2^3 - \frac{1}{3})^{1/2} \right] \quad (58)$$

In the high electric field limit the first term under the square root will dominate, and therefore, using (45),

$$\bar{v}_2 = v_L + (e/2\beta \hbar k_0)^{1/2} E^{1/2} \quad (59)$$

determines the limiting behaviour of $\bar{v}_2(E)$ for two-roton emission.

rev

Assuming again that $m_i = 72m_4$, we find that $\Delta v_2 = 2\Delta v_1 = 8.9 \text{ ms}^{-1}$. Thus for $\bar{v} < 55 \text{ ms}^{-1}$ we might expect our data to be described by (51) whereas, for higher velocities, it will be necessary to use (58). In fact in our highest electric field of 300 kV m^{-1} we find $\bar{v} = 57 \text{ ms}^{-1}$, so that (51) should be applicable throughout our whole experimental range. Of course, if the ionic mass was larger than $72m_4$, we would then expect to observe small deviations from (51) at the high velocity end of the characteristic.

fig 17

We compare some of our experimental results with (51) by plotting \bar{v} against $E^{1/3}$ in figure 17. It is evident that straight lines may be drawn through most of the data, although there appear to be deviations in the limits of high and low electric fields. The full lines represent least-squares fits of the data in the figures to the equation

$$\bar{v} = v_L + A E^{1/3} \quad (60)$$

within the ranges indicated, treating both v_L and A as adjustable parameters. The values of v_L obtained in this way, of 46.3 ms^{-1} from the 0.35K data and 46.1 ms^{-1} from the 0.45K data, are in excellent agreement with the value of 45.6 ms^{-1} computed from the Landau parameters using (13), considering that our systematic experimental uncertainty is $\pm 3\%$ in \bar{v} .

Drawing similar plots for a number of temperatures we have found that the deviation at low values of E is apparently temperature independent for $T < 0.35\text{K}$, which



suggests that it is associated with the scattering of ^3He isotopic impurities. At higher temperatures, as can be seen in figure 17(b), the deviation becomes larger, and extends to larger values of E , as would be expected if the drag arising from phonon scattering were becoming more significant.

The small deviations from (60) above 200 kV m^{-1} are independent of temperature and might, perhaps, be a consequence of v_{F2} becoming larger than v_2' (see figure 16) so that (58) will be the relevant equation rather than (51). It is of interest to try and compute what value of the ionic effective mass would give rise to the deviations which we observed. In figure 18 we have plotted a portion of our averaged (see below) high field data on a larger scale. The dashed curves represent the behaviour expected for ions of various masses, using (58) and obtaining an experimental value of $A = 3e/\beta m_{ij}$ by fitting (51) to the data at lower values of E . Unfortunately, the observed deviations are rather small compared to the size of our experimental errors, but we may certainly conclude that the ionic mass is less than $150m_4$; and, while no firm conclusion can be drawn from the present experimental results, it rather looks as though our estimate of $m_{ij} = 72 m_4$ may turn out to be an underestimate.

It is clear that further experiments extending to higher electric fields may be expected to yield a measure of the ionic mass in superfluid helium under pressure. We note however that a more sophisticated analysis might then

Figure 18



be required. For example, the possibility of emission processes involving three or more excitations should perhaps also be considered; and, for very large values of \bar{v} , it might become necessary to take explicit account of departures of $\epsilon(k)$ from the simple parabolic relations (5) which we assumed above.

Supposing, in the absence of firm evidence to the contrary, that our estimate of $72 m_4$ for the ionic mass is correct, we can use (44), (51) and (57) in conjunction with our data to deduce a numerical value for V_{k_0, k_0} . In doing so, we have noted that the appropriate value of v to insert in (44) is the ionic velocity at which, on average, the emission events occur, $v_{e2} (= \bar{v}_2 + \hbar k_0 / m_i)$. We find $V_{k_0, k_0} = (3.6 \pm 0.7) \times 10^{-52} \frac{\text{J}}{\text{m}^3}$, where the error limits refer to uncertainties of: $\pm 5\%$ in measuring A ; $\pm 1\%$ in k_0 ; $\pm 5\%$ in m_i ; and $\pm 15\%$ in m_i , based on an estimated uncertainty of $\pm 5\%$ in

r_i . In carrying out the computation we have introduced an additional multiplicative factor of 0.893 within the parentheses on the right hand side of (48) in order, as discussed above, to correct the equation in the light of Bowley and Sheard's more rigorous version of the theory. To obtain the most reliable values of A and v_L in (60) we have incorporated almost all our data below 0.5 kV : in order to eliminate the influence of excitation scattering in low electric fields at the higher temperatures, however, we have omitted points below 7.5 kV m^{-1} in the case of 0.4 kV and 0.45 kV data, and below 15 kV m^{-1} in the case

of the 0.5K data. This procedure, which effectively averages a very large body of data recorded by different experimenters on different occasions, should have helped to minimise the biasing influence of the small systematic errors which might, for example, have arisen from a particular experimenter's style of measuring up the pulses on the point-plotter recordings. We find: $v_L = (46.30 \pm 0.04) \text{ ms}^{-1}$; $A = (0.144 \pm 0.002) \text{ ms}^{-1} (\text{V m}^{-1})^{1/2}$; where the quoted errors refer only to the statistical confidence with which we can fit (60) to the data (the $\pm 3\%$ uncertainty in ℓ introduces an additional systematic error of up to $\pm 5\%$ in A); and the above estimate of $\sqrt{V_{k_0, k_0}}$ is based on these values. It would, of course, be possible to try and reduce the systematic error in A arising from the 3% uncertainty in ℓ by adjusting the value of ℓ used to compute E and \bar{v} to be such that the intercept on the velocity axis, in a plot such as those of figure 17, was precisely equal to the value of v_L computed from the roton parameters. In view of the $\pm 15\%$ uncertainty in m_0 , however, we have not felt this procedure to be justified at present, especially since the experimental intercepts are in any case within about 1.5% of v_L .

We can try to obtain a rough estimate of the error introduced by our having ignored the variation ($\pm 7\%$ for the range of E within which we fitted our data to equation 51) of the average velocity of emission, v_{e2} , which we used for v in the denominator of (44), by rewriting the corrected (51) in the form

$$\bar{v}_2 = v_L + \gamma \frac{v_{e2}^2}{v_{e2}^3} E^{1/3},$$



where

$$\gamma = (0.893 \times 6\pi^2 \hbar^3 e/k_0^4 |V_{k_0, k_0}|^2 m_e m_i)^{1/3}$$

and then plotting \bar{v} against $v_{e2}^{2/3} E^{1/3}$ to obtain the gradient γ . We again obtain an excellent straight line within the scatter of the data from which we deduce $V_{k_0, k_0} = 3.8 \times 10^{-52} \text{ J m}^3$. Of course, this procedure is hardly rigorous because, properly, we should consider the effect of changes in v_{e2} under the integral in (48); but it is reassuring that we still obtain a straight line plot, and that the value of V_{k_0, k_0} obtained in this way differs from the value derived on the assumption of a constant β by an amount smaller than the other uncertainties in the measurement.

To try and ascertain whether our experimental value of the matrix element is reasonable, we have calculated the T matrix in the ladder approximation (Bowley, to be published), assuming an interaction which is large and independent of angle. To the lowest order in quantities like $k_0/m_i v$, we find

$$|T_{k_0, k_0}|^2 \approx \frac{(\pi^2 \hbar^3 v)^2}{m_i k_0^3 [1 + (v - v_L - \hbar k_0/m_i)/2v_L]} \quad (61)$$

If we assume

Assuming $v = 55 \text{ m s}^{-1}$, $m_i = 72m_4$, this yields

$T_{k_0, k_0} = 2.9 \times 10^{-52} \text{ J m}^3$. In view of the approximations inherent in the calculation, this represents good agreement with our experimental value of $3.6 \times 10^{-52} \text{ J m}^3$ for V_{k_0, k_0} ;

and the relatively weak dependence on v in (61) (which is actually in such a direction that it would tend to diminish the velocity dependence of A in (60)) provides some encouraging support for our assumption, in calculating $R_2(v)$, that the matrix element could to a first approximation be considered velocity independent. It is also reassuring that (61) predicts a matrix element which varies very weakly with pressure: this again is consistent with experiment in that the value of A derived from data recorded at different pressures turns out to be almost independent of pressure.

We have also tried to fit some of our data for lower pressures to (60). Because the ratio of the Landau parameters (Δ/k_0) increases with falling pressure, (7) implies that v_L should also increase. Unfortunately the decrease in signal *intensity* with falling pressure prevents any satisfactory comparison of the experimental and calculated values of v_L . The difficulty arises partly because the data are noisier, but mainly because the threshold electric field, below which the signal becomes undetectable, increases as the pressure is reduced. Thus to obtain a value of v_L by fitting the data to (60) at the lower pressures entails extrapolating noisy data in a narrow range of $E^{1/3}$, on a plot such as those of figure 17, over a long span. The results are shown in figure 19,

Figure 19



where we compare the measured values $v_L(P)/v_L(25 \times 10^5)$ with those calculated from the roton parameters. It seems clear that v_L does indeed increase with falling pressure, but a satisfactory quantitative comparison of theory and experiment below 23×10^5 Pa is clearly impossible.

Noting that our data are consistent with (57) over a very wide range of electric fields (E changing by a factor of 100), and that the values of v_L deduced from the data increase with decreasing pressure, we conclude that our experimental results amount to an impressive confirmation of the applicability of Bowley and Sheard's (1975) two-roton emission theory.

(f) Is the single-roton emission process forbidden?

The comparison of our experimental data with Bowley and Sheard's (1975) theory in §§ 4²²(d) and (e) seems to demonstrate unequivocally that, under our experimental condition, the superfluidity of liquid ⁴He breaks down through the emission of rotons in pairs rather than singly. This result is surprising. There was no obvious reason, on the basis of our present understanding of rotons, to predict such an effect in advance of the experiment; neither can we, even in retrospect, offer any physical explanation of the phenomenon. If the single-roton process is, for some reason at present unknown, forbidden, then this fact probably amounts to an important piece of evidence concerning the physical nature of rotons. Before completely accepting the two-roton hypothesis, therefore, it is essential to consider whether there is any plausible

alternative explanation for our experimental results.

It is, of course, possible that the theory outlined above is wrong or inapplicable for some reason. Perhaps the excitations which are generated by the ion may not be rotons at all but might, for example, be vortex rings? It is true, after all, that some of the ions apparently create, and become trapped by, vortex rings before they reach the collector (McClintock & Phillips, 1975). This suggestion seems implausible, however, when we note that the critical velocity at which dissipation ^{starts} commences is found experimentally to be the Landau critical velocity for roton creation: this is evident even on a plot such as that of figure 11, where we have made no assumptions at all about the way in which the superfluidity is breaking down. Furthermore, values of v_L extracted from the data using (60) show an increase with falling pressure (figure 19), whereas the critical velocity for vortex nucleation by a negative ion is known to decrease as the pressure is reduced (Schwarz & Jang, 1973). It seems extremely likely, therefore, that the dissipative mechanism which prevents the ions from accelerating much beyond v_L is, as we have assumed, the emission of rotons.

Another possibility is that one-roton emission is, as was originally envisaged, the dominant mechanism but that, because we have failed to take account of some vital factor, (57) does not as it stands provide a correct description of the phenomenon. The matrix element V_k which enters (32) through α and (19) might, for example, be velocity dependent in just such a manner as to change the behaviour from the

Small fractions expected $\frac{2}{3}$ law to a $\frac{1}{3}$ power law in $(\bar{v}-v_L)$, thus rendering a spurious resemblance to the two-roton formula (51). It would certainly represent a remarkable coincidence if this were so, considering the very large range of E ($2 < E < 200 \text{ kV/m}^{-1}$) over which (51) is accurately obeyed and, although the possibility cannot be entirely discounted, we feel that it is far more likely that the two-roton theory is in fact correct.

The probable applicability of the two-roton hypothesis over the range of our experiments does not, however, necessarily imply that one-roton processes are rigorously forbidden. The matrix element V_k may be very small relative to $V_{q,k}$ so that, in a time less than τ_1 , the ion accelerates beyond v_2' and emits a pair of rotons. Of course, by reducing the electric field we can increase the time taken by the ion to accelerate from v_1' to v_2' , and thus increase the likelihood of single-roton emission. Single-roton processes, if they exist at all, are most likely to be found occurring under very small electric fields, in the region below 2 kV m^{-1} where, in the present experiments, any such effects would be obscured by the scattering of ^3He isotopic impurities and thermal excitations.

Although we cannot, of course, derive a numerical value of V_{k_0} from the present experimental data we can, however, deduce an upper limit for the magnitude of this matrix element. We note that the lowest electric field for which our data lie accurately on a plot such as that of figure 17 is about 2 kV m^{-1} and so we can be confident that the average pre-emission period τ_1 (assuming $t = 0$ at $v = v_1'$) for the one roton process is certainly considerably longer

than the time taken for the ion to accelerate from v_1' to v_2' in this electric field. Then, using (24) for τ_1 ,

$$(3/2\alpha)^{2/3} (m_1/eE)^{1/3} > (v_2' - v_1') / (eE/m_1)$$

Noting from figures 14 and 16 that $(v_2' - v_1') = \hbar k_0 / 2m_1$, and substituting for α from (19), we obtain

$$|V_{k_0}|^2 < 3\hbar v_e m_1^{1/2} eE / m_1^{1/2} k_0^3$$

from which, for $E = 2 \text{ kV} \text{ m}^{-1}$, we find

$$V_{k_0} < 6 \times 10^{-39} \text{ Jm}^{3/2}$$

If, in future experiments at lower temperatures and using isotopically purer ^4He , (51) continues to be followed down to smaller electric fields, then it will be possible to reduce the upper bound on V_{k_0} yet further. If, on the other hand, the matrix element is in fact nonzero, then $\bar{v}(E)$ will take the form of (26) for sufficiently small E and the experiments might then enable a numerical value of V_{k_0} to be deduced.

5. Conclusion

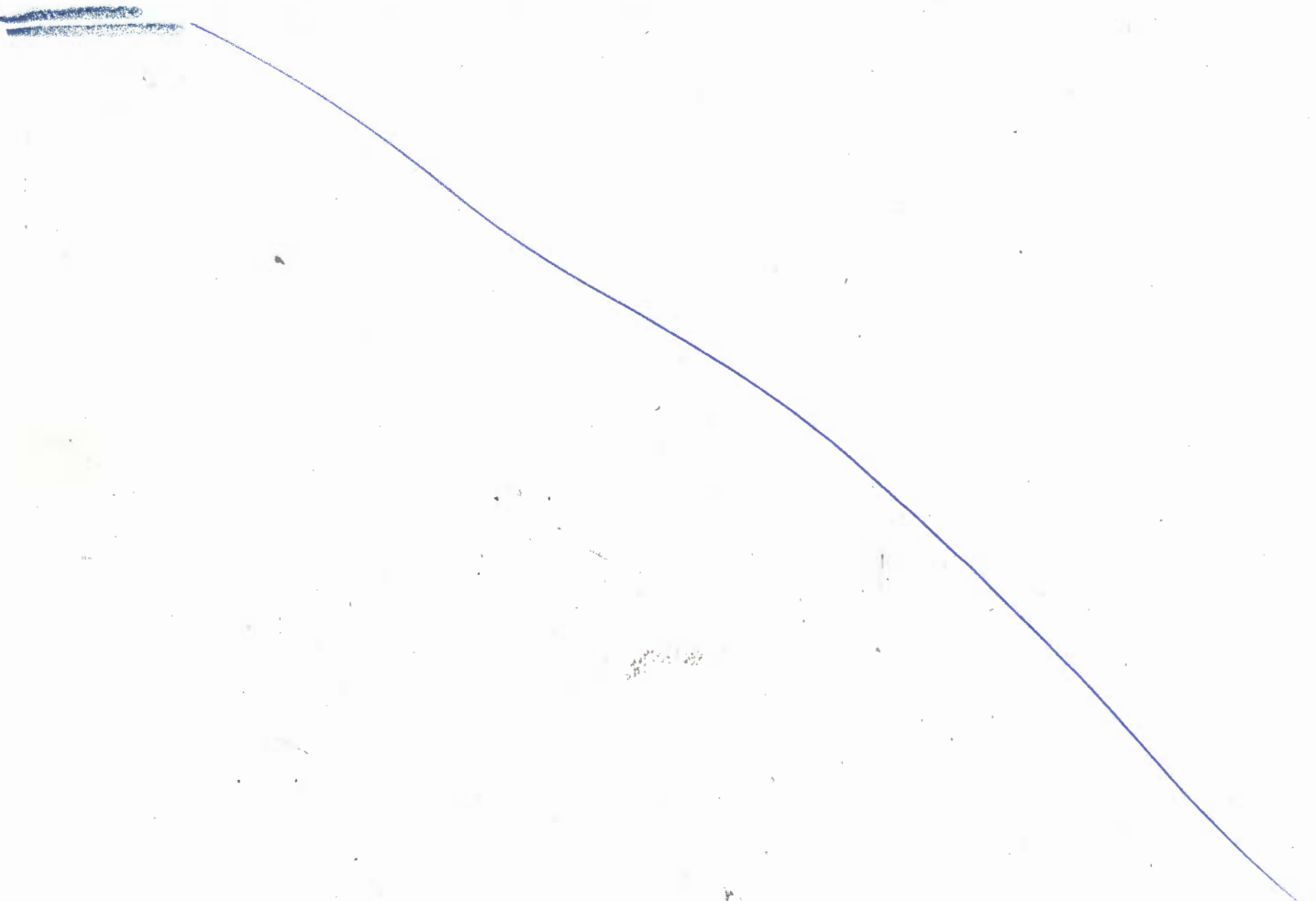
The experiments which we have described constitute the first convincing verification of Landau's (1941, 1947) explanation of superfluidity in liquid ^4He .

We have shown that Takken's (1970) wave radiation model has led to a gross overestimate of the drag on an ion travelling through the superfluid faster than the Landau critical velocity for roton creation and, furthermore, that it has given rise to an incorrect prediction of the form of the $\bar{v}(E)$ relationship. We have, however, demonstrated that, over a very wide range of electric fields, our measurements are accurately described by a law of the form $(\bar{v}-v_L) \propto E^{1/3}$, in agreement with the two-roton theory of Bowley and Sheard (1975). On the basis of their theory we have deduced a numerical value of the matrix element characterising the two-roton emission process.

math sign No sign of the $(\bar{v}-v_L) \propto E^{2/3}$ behaviour, which, according to the Bowley and Sheard theory, characterises single-roton emission is evident from our data, so that we have not been able to determine the relevant matrix element: we have, however, placed an upper bound on its value. Single-roton processes, if they exist, are likely to be observed for very weak electric fields in the region where, in our present work, the phenomenon would be obscured by the presence of excitation and impurity scattering processes: experiments at lower temperature, using purer ^4He , are clearly required to try and settle the interesting question

of whether such emission processes can occur in reality.

H It is a pleasure to acknowledge helpful discussions or correspondence with Dr/ A.J. Leggett, Dr/ D.A. Neep, Dr/ T.C. Padmore, Dr/ G.R. Pickett and Dr/ E.H. Takken. We are also very grateful to Dr/ F.W. Sheard for his encouragement and help, to Mr/ N. Bewley who built the cryostat and constructed the experimental chamber, and to Mr/ D.H. Bidle and Mr/ R.O. Makin who designed and built the e.h.t. pulse generator. The experimental work was supported by the Science Research Council (under B/RG/6094.8) to whom two of us (D.R.A. and A.P.) are also indebted for the assistance of studentships.



Appendix A : Tabular Velocity Data

Most of the data were recorded ^{with} a pressure of 25×10^5 Pa which resulted in relatively large signals, which could quickly be averaged to a satisfactory signal/noise ratio and measured up with a precision of about ± 1 or 2% . We list these first, for five different temperatures and a very full set of electric fields, in table ^{A1} 2. In table ^{A2} 3 we list data recorded at 21×10^5 Pa, for three temperatures and a restricted range of electric field above about 100 kV m^{-1} . A few data were also recorded at 22×10^5 Pa and 23×10^5 Pa, all at 0.28K , and are listed in table ^{A3} 4. Finally we tabulate in table ^{A4} 5, for four temperatures, the drift velocity as a function of pressure under a field of about 100 kV m^{-1} . Whenever more than one datum is available for a particular set of (P, E, T), we have tabulated the average value.

vom D

In all cases we give not the electric field, but the potential difference V_D measured across the drift space. The length of the drift space, as discussed in § 3(c), was $10.2 \pm 0.3\text{mm}$ [#] so that the electric field E _(in kV m^{-1}) may be found by multiplying the numerical value of V_D by 0.098 . The uncertainty in l introduces possible systematic errors of $\pm 3\%$ in E (to which must be added the $\pm 2\%$ error in measuring V_D) and $\pm 3\%$ in \bar{v} ; random errors in the measurements manifest themselves as a scatter in the data.

LOW DECIMAL

Table 2, Velocity data at 25×10^5 Pa

The measured ionic drift velocities are given in ms^{-1} for various temperatures T and drift space potential differences V_D .

V_D (V)	T (K)	0.30	0.35	0.40	0.45	0.50
10	10m	-	46.2	45.8	42.0	-
11		-	-	45.7	43.0	-
12		-	46.5	45.8	43.2	-
13		-	46.8	46.1	43.8	39.4
14		-	46.8	46.4	44.2	40.4
15		-	47.3	47.2	44.6	41.0
16		-	47.3	46.8	44.9	41.2
17		-	-	46.9	45.4	41.5
17.5		-	47.6	-	-	-
18		-	-	47.0	45.5	42.7
18.5		-	47.5	-	-	-
19		-	-	-	45.8	42.7
20		47.7	47.9	47.5	46.3	43.2
21		47.3	47.7	47.4	46.0	43.5
22		-	-	47.0	46.5	43.8
22.5		47.4	48.0	-	-	-
23		-	-	47.6	46.1	44.0
24		-	-	47.6	46.6	44.5
25		47.9	48.0	47.7	46.8	44.7
26		-	-	47.9	46.9	44.8
27		-	-	48.0	47.0	45.1
27.5		47.9	48.1	-	-	-
28		-	-	48.0	46.9	45.2
29		-	-	48.1	47.2	45.6
30		48.3	48.3	48.2	47.3	45.8
32.5		48.0	48.3	48.1	47.3	46.1
35		48.3	48.4	48.1	47.6	46.2
37.5		48.1	48.6	48.3	47.4	46.6
40		48.7	48.7	48.5	48.0	46.9
42.5		48.6	-	-	-	47.0
45		48.6	48.7	48.6	48.0	47.3
47.5		48.6	-	-	-	47.3
50		48.6	48.9	48.8	48.4	47.6
52.5		48.7	-	-	-	-
55		48.7	48.9	48.9	48.6	47.7
57.5		49.0	-	-	-	-
60		49.3	48.9	48.9	48.4	47.7
62.5		49.0	-	-	-	-
65		49.3	49.0	48.9	48.7	48.1
70		49.0	49.3	49.2	48.9	48.0
75		49.5	49.0	49.1	48.9	48.3
80		49.3	49.5	49.3	48.9	48.6

Continued

Centre
↑
from
of rules
low dec

T/K

repeat leads as necessary

Table 2 (continued)

V_D (V) \ T (K)	0.30	0.35	0.40	0.45	0.50
85	49.5	49.2	49.3	49.0	48.6
90	49.2	49.5	49.5	49.3	48.7
95	49.6	49.3	49.5	49.2	48.7
100	49.8	49.5	49.4	49.3	48.9
110	50.1	49.8	49.8	49.5	49.2
120	50.1	49.6	49.6	49.5	49.2
125	-	-	49.5	-	-
130	50.1	49.8	49.9	49.6	49.3
140	50.2	49.9	49.8	-	49.3
150	50.4	49.8	50.0	49.8	49.5
160	50.5	49.9	49.9	-	49.5
170	50.2	-	50.2	50.1	49.5
175	-	50.2	-	-	-
180	50.5	-	50.1	49.9	49.6
185	-	50.1	-	-	-
190	50.4	-	50.2	-	49.6
200	50.4	50.4	50.2	50.1	49.9
210	50.7	-	-	-	-
220	50.7	-	-	-	50.1
225	-	50.4	50.5	50.2	-
230	51.0	-	-	-	-
240	50.5	-	-	-	50.1
250	50.7	50.5	50.6	50.2	-
260	50.7	-	-	-	50.1
270	51.0	-	-	-	-
275	-	50.5	50.8	50.5	-
280	50.7	-	-	-	50.4
290	50.8	-	-	-	-
300	51.0	50.8	50.7	50.5	50.2
325	50.8	50.7	51.0	50.8	50.4
350	51.2	51.2	51.2	50.8	50.5
375	51.2	51.3	51.2	50.8	50.8
400	51.5	51.3	51.2	51.2	50.7
425	-	51.3	51.2	-	-
450	51.5	51.7	51.5	51.3	51.2
475	-	51.5	51.5	-	-
500	51.8	51.7	51.5	51.3	51.2
525	-	-	51.7	-	-
550	51.7	52.0	52.0	51.8	51.5
575	-	-	51.8	-	-
600	52.0	51.8	52.0	51.8	51.7
625	-	-	52.1	-	-
650	52.0	52.1	52.1	52.0	51.7
675	-	-	52.1	-	-
700	52.1	52.5	52.3	52.0	51.8
750	52.3	52.7	52.4	52.3	52.1
800	52.5	52.7	52.5	52.3	52.0
850	52.5	52.8	52.7	52.5	52.5
900	52.5	52.8	52.8	52.5	52.7
950	52.7	53.0	53.2	52.8	52.1
1000	52.8	53.0	52.9	52.8	52.7

*87 miles
low dec*

continued



repeat leads as necessary

Table 2 (continued)

$T(K) \backslash V_D(V)$	0.30	0.35	0.40	0.45	0.50
1100	53.0	53.3	53.3	53.0	53.0
1200	53.2	53.9	53.3	53.2	53.0
1300	53.3	53.9	53.9	53.5	53.3
1400	53.5	53.9	53.9	53.7	53.7
1500	53.7	54.2	54.1	53.8	53.9
1600	53.9	54.2	54.0	54.0	54.0
1700	54.2	54.6	54.6	54.0	53.9
1800	54.2	54.6	54.8	54.2	54.0
1900	54.4	54.8	55.0	54.4	54.2
2000	54.4	55.0	54.9	54.6	54.2
2100	54.6	55.0	55.1	54.8	54.4
2200	55.0	55.1	55.1	55.0	54.6
2300	55.1	55.3	55.5	55.0	54.8
2400	55.1	55.7	55.5	55.3	55.1
2500	55.3	55.7	55.8	55.3	55.1
2600	55.3	55.9	55.9	55.5	55.7
2700	55.7	56.1	55.9	55.7	55.3
2800	55.7	56.1	56.1	55.9	55.5
2900	55.7	56.5	56.3	55.9	55.9
3000	55.9	56.5	56.4	56.3	55.9

9

9 rules
low dec

Table 3. Velocity data at 21×10^5 Pa

(The measured ionic drift velocities are given in ms^{-1} for various temperatures T and drift space potential differences V_D .)

T/K	T/K		
V_D/V	0.29	0.33	0.37
1000	55.9	-	-
1200	56.1	56.4	55.9
1250	56.7	56.0	-
1300	56.5	56.5	56.3
1350	56.5	56.6	56.0
1400	56.5	56.4	56.3
1450	56.7	56.4	56.2
1500	57.1	56.5	56.6
1550	56.9	56.7	56.6
1600	57.3	56.7	56.5
1650	57.1	56.9	56.8
1700	57.3	57.1	56.9
1750	57.3	56.9	56.9
1800	57.7	57.7	57.3
1850	57.7	57.1	56.8
1900	57.7	57.7	57.5
1950	57.5	57.7	57.1
2000	58.5	57.9	57.7
2050	57.9	57.7	-
2100	58.3	58.1	57.6
2150	58.5	57.7	57.5
2200	58.3	58.3	57.9
2250	58.7	-	-
2300	58.7	58.1	58.3
2350	58.7	58.5	57.7
2400	58.7	58.7	58.3
2450	58.9	-	-
2500	58.7	58.7	58.3
2550	58.7	58.9	58.8
2600	59.1	58.5	58.3
2650	-	-	-
2700	59.1	58.9	58.8
2750	59.1	59.1	58.7
2800	59.4	58.7	58.7
2850	-	-	-
2900	59.4	59.1	58.7
2950	59.1	59.1	58.7
3000	59.6	59.1	59.1

of rules
low dec

$10^{-5} P/Pa$

Table 4. Velocity data at 22×10^5 and 23×10^5 Pa

The measured ionic drift velocity at a temperature of $0.28K$ is given in ms^{-1} for various drift space potential differences V_D .

rules
low dec

$10^5 P / Pa$	22	23
500	-	52.3
550	-	53.0
600	-	52.8
650	-	53.2
700	-	53.3
750	-	53.5
800	54.4	53.5
850	54.4	53.7
900	54.8	53.9
950	55.0	53.9
1000	55.1	54.0
1100	55.3	54.2
1150	55.0	-
1200	55.3	54.4
1300	55.5	54.6
1350	55.7	-
1400	55.5	54.8
1500	55.9	55.0
1550	55.7	-
1600	55.9	55.1
1650	56.3	-
1700	56.4	55.5
1750	56.3	-

$10^5 P / Pa$	22	23
1800	56.3	55.5
1850	56.5	-
1900	56.3	55.7
1950	56.5	-
2000	56.5	55.7
2050	56.5	-
2100	56.5	55.9
2150	57.1	-
2200	57.1	56.1
2250	56.9	-
2300	57.1	56.3
2350	57.5	-
2400	57.3	56.5
2450	57.1	-
2500	57.1	56.5
2550	57.3	-
2600	57.5	56.5
2650	57.3	-
2700	57.5	56.7
2750	57.7	-
2800	57.7	56.7
2850	57.3	-
2900	57.5	56.9
2950	57.5	-
3000	57.7	56.9

$$10^{-5} P / \text{Pa}$$

A4

Table 5. Velocity as a function of pressure.

The measured ionic drift velocity with a drift space potential difference of 1000 V is given in ms^{-1} for various temperatures T and pressures P.)

T (K) P (10^{-5} Pa)	0.29	0.35	0.40	0.50
20.25	-	-	-	55.9
20.50	57.7	-	-	55.9
20.75	57.1	-	-	55.7
21.00	56.2	54.8	56.5	55.7
21.25	55.7	55.9	56.1	55.5
21.50	55.7	55.7	55.7	55.3
21.75	55.0	55.5	55.7	55.1
22.00	55.1	55.3	55.1	55.1
22.25	55.0	55.1	55.0	54.8
22.50	54.8	55.0	54.8	54.6
22.75	54.6	54.4	54.4	54.4
23.00	54.6	54.2	54.4	54.4
23.25	54.4	54.2	54.0	54.2
23.50	53.9	54.0	54.0	54.0
23.75	54.0	54.0	53.7	53.9
24.00	53.8	53.7	53.9	53.7
24.25	53.7	53.7	53.3	53.5
24.50	53.3	53.7	53.3	53.3
24.75	53.3	53.3	53.0	53.2
25.00	52.9	53.0	53.0	52.9

Center
of rules
has dec

Appendix II : The single roton transition rate

To calculate the velocity dependence of the single-roton transition rate, starting from

$$R_1(v) = \frac{2\pi}{h} \sum_{\mathbf{k}} |V_{\mathbf{k}}|^2 \delta(\epsilon + \hbar^2 k^2 / 2m_1 - \hbar \mathbf{k} \cdot \mathbf{v}) \quad (17)$$

we replace the sum over all accessible final states by an integral, so that

$$R_1(v) = \frac{2\pi}{h} \left(\frac{1}{2\pi}\right)^3 \int_0^\infty dk k^2 \int_0^{2\pi} d\phi \int_{-1}^1 d(\cos\alpha) |V_{\mathbf{k}}|^2 \delta(\epsilon + \hbar^2 k^2 / 2m_1 - \hbar k v \cos\alpha)$$

where α is the angle between \mathbf{v} and \mathbf{k} . The integral over ϕ is trivial owing to the cylindrical symmetry of the problem. Setting $\cos \alpha = x$ and assuming that $V_{\mathbf{k}}$ is a constant ($= V_{k_0}$) within the range of interest,

$$R_1(v) = \frac{|V_{k_0}|^2}{2\pi h} \int_0^\infty dk k^2 \int_{-1}^1 dx \delta(\epsilon - \hbar^2 k^2 / 2m_1 - \hbar k v x)$$

Integrating over x ,

$$R_1(v) = \frac{|V_{k_0}|^2}{2\pi h} \int_0^\infty dk k^2 (\hbar v k)^{-1} \theta(\hbar v k - \epsilon - \hbar^2 k^2 / 2m_1)$$

where θ is the unit step function. Before performing the final integration it is convenient to change the variable from k to ϵ , using (5). In doing so we introduce a factor of 2 to take account of there being two values of k associated with each value of ϵ ; and we ignore $[2m_r(\epsilon - \Delta)]^{1/2}$ in comparison with k_0 . Then,

$$R_1(v) = \frac{k_0 |V_{k_0}|^2}{\pi \hbar^3 v} \int_{\Delta}^{\infty} [2(\epsilon - \Delta)/m_r]^{-1/2} d\epsilon \theta(\hbar v k_0 - \epsilon - \hbar^2 k_0^2 / 2m_1)$$

upright pi pi
Σ

mid pt

-k

slowing Δ

Setting $\epsilon - \Delta = s$, we obtain

$$R_1(v) = \frac{k_0 |V_{k_0}|^2 (m_p/2)^{1/2}}{\pi \hbar^3 v} \int_0^\infty s^{-1/2} \theta(\hbar v k_0 - \hbar^2 k_0^2 / 2m_1 - s - \Delta) ds$$

Because the integral is nonzero only when

$$s < \hbar v k_0 - \hbar^2 k_0^2 / 2m_1 - \Delta = a,$$

we can write

$$R_1(v) = \frac{k_0 |V_{k_0}|^2 (m_p/2)^{1/2}}{\pi \hbar^3 v} \int_0^a s^{-1/2} ds.$$

Integrating, and noting from (7) and (14) that $a = \hbar k_0 (v - v_1')$ to an excellent approximation for an ion of mass $72m_4$, we obtain finally

$$R_1(v) = \frac{|V_{k_0}|^2 (2m_p)^{1/2} k_0^{3/2}}{\pi \hbar^{5/2} v} (v - v_1')^{1/2}. \quad (18, 19)$$

Appendix III : the two roton transition rate

To calculate the velocity dependence of the two-roton transition rate, starting from

mid pt

$$R_2(v) = \frac{2\pi}{\hbar} \sum_{\underline{k}} \sum_{\underline{q}} |V_{\underline{k}, \underline{q}}|^2 \delta \left[\epsilon_{\underline{k}} + \epsilon_{\underline{q}} - \hbar(\underline{k} + \underline{q}) \cdot \underline{v} + \hbar^2 (\underline{k} + \underline{q})^2 / 2m_1 \right] \quad (39)$$

we replace the sums over \underline{k} and \underline{q} by integrals such that

mid pt

$$\sum_{\underline{k}} \rightarrow \frac{1}{(2\pi)^3} \int d\underline{k} k^2 \int_0^{2\pi} d\phi \int_{-1}^1 d(\cos \alpha)$$

and

$$\sum_{\underline{q}} \rightarrow \frac{1}{(2\pi)^3} \int d\underline{q} q^2 \int_0^{2\pi} d\phi \int_{-1}^1 d(\cos \beta),$$

where α and β are the angles between \underline{v} and \underline{k} , and \underline{v} and \underline{q} , respectively. Because k and q in the roton region are close to k_0 , and α and β are small, we can take $(\underline{k} + \underline{q})^2 \approx 4k_0^2$ and $(\underline{k} + \underline{q}) \cdot \underline{v} \approx k_0 v (\cos \alpha + \cos \beta)$ to excellent approximations. The ϕ integrals each yield a factor of 2π owing to the cylindrical symmetry of the problem. Setting $\cos \alpha = x$, $\cos \beta = y$, and assuming that $V_{\underline{k}, \underline{q}}$ is a constant ($= V_{k_0, k_0}$) over the ionic velocity range of interest, we find

$$R_2(v) = \frac{|V_{k_0, k_0}|^2}{(2\pi)^3} \int d\underline{k} \int d\underline{q} k^2 q^2 \int_{-1}^1 dx \int_{-1}^1 dy \delta \left[\epsilon_{\underline{k}} + \epsilon_{\underline{q}} + 2\hbar^2 k_0^2 / m_1 - \hbar v k_0 (x+y) \right]$$

We first perform the y integration, noting that

$$\int_{-1}^1 dy \delta(a-by) = |b^{-1}| \theta(b-a),$$

where a and b are constants and θ is again the unit step function. Then

$$R_2(v) = \frac{|V_{k_0, k_0}|^2}{\hbar^3 (2\pi)^3} \int dk k^2 \int dq q^2 \int_{-1}^1 dx (\hbar v q)^{-1} \theta[\hbar v k_0 + \hbar v k_0 x - \epsilon_k - \epsilon_q - 2\hbar^2 k_0^2 / m_i]$$

The x integral is (because of the θ function and the upper limit) to be evaluated only within the region

$$B = (-\hbar v k_0 + \epsilon_k + \epsilon_q + 2\hbar^2 k_0^2 / m_i) / \hbar v k_0 \leq x \leq 1,$$

so that

$$R_2(v) = \frac{|V_{k_0, k_0}|^2}{\hbar^2 v (2\pi)^3} \int dk k^2 \int dq q^2 \int_B dx$$

yielding

$$R_2(v) = \frac{|V_{k_0, k_0}|^2}{\hbar^3 v^2 (2\pi)^3} \int dk k \int dq q \left\{ 2\hbar v k_0 - \epsilon_k - \epsilon_q - 2\hbar^2 k_0^2 / m_i \right\}$$

We note that this expression is symmetrical in q and k, as is required by the model; and that the expression in curly brackets must be positive since, otherwise, we would be considering $x > 1$. To take account of the latter requirement, we multiply the right hand side of the equation by the θ function of the expression in curly brackets. It is convenient, before attempting the remaining integrations, to change the variables from k and q to the energies ϵ_k, ϵ_q of the emitted rotons, using (5). In doing so we must introduce a factor of 2 in each case in order to take account of the

two k or q values associated with each energy. We obtain

$$R_2(\nu) = \frac{2k_0^2 |V_{k_0, k_0}|^2 m_r}{\hbar^5 \nu^2 (2\pi)^3} \int_{\Delta}^{\infty} d\epsilon_k \int_{\Delta}^{\infty} d\epsilon_q (\epsilon_k - \Delta)^{-\frac{1}{2}} (\epsilon_q - \Delta)^{-\frac{1}{2}}$$

$$\theta(2\hbar\nu k_0 - 2\hbar^2 k_0^2/m - \epsilon_k - \epsilon_q) \theta(2\hbar\nu k_0 - 2\hbar^2 k_0^2/m_1 - \epsilon_k - \epsilon_q)$$

Setting $s = \epsilon_k - \Delta$, $t = \epsilon_q - \Delta$

$$R_2(\nu) = \frac{2k_0^2 |V_{k_0, k_0}|^2 m_r}{\hbar^5 \nu^2 (2\pi)^3} \int_0^{\infty} ds \int_0^{\infty} dt s^{-\frac{1}{2}} t^{-\frac{1}{2}} (2\hbar\nu k_0 - 2\hbar^2 k_0^2/m_1 - s - t - 2\Delta)$$

$$\theta(2\hbar\nu k_0 - 2\hbar^2 k_0^2/m_1 - s - t - 2\Delta)$$

Taking account of the ~~theta~~ function, and of the lower limit of integration, we see that the t integral is to be evaluated only in the region $0 < t < b - s$ where

$$b = 2\hbar\nu k_0 - 2\hbar^2 k_0^2/m_1 - 2\Delta;$$

and that the limits of the s integration therefore become $0 < s < b$, because, if $s > b$, t would be negative.

Thus

$$R_2(\nu) = \frac{2k_0^2 |V_{k_0, k_0}|^2 m_r}{\hbar^5 \nu^2 (2\pi)^3} \int_0^b ds \int_0^{b-s} dt s^{-\frac{1}{2}} t^{-\frac{1}{2}} (b-s-t)$$

The t integration is straightforward, yielding

$$R_2(\nu) = \frac{2k_0^2 |V_{k_0, k_0}|^2 m_r}{\hbar^5 \nu^2 (2\pi)^3} \int_0^b ds s^{-\frac{1}{2}} \frac{4}{3} (b-s)^{3/2}$$

Integrating by parts,

$$R_2(v) = \frac{8k_0^2 |V_{k_0, k_0}|^2 m_r}{\hbar^5 v^2 (2\pi)^3} \int_0^b ds s^{\frac{1}{2}} (b-s)^{\frac{1}{2}},$$

which, setting $s = bz$, becomes

$$R_2(v) = \frac{8k_0^2 |V_{k_0, k_0}|^2 m_r}{\hbar^5 v^2 (2\pi)^3} b^2 \int_0^1 dz z^{\frac{1}{2}} (1-z)^{\frac{1}{2}}$$

The integral is now in a standard form taking the value $\frac{\pi}{8}$.

Using (7) and (39), we note that $b = 2\hbar k_0 (v - v_1')$ so that we obtain finally

$$R_2(v) = \frac{k_0^4 |V_{k_0, k_0}|^2 m_r}{2\pi^2 \hbar^3 v^2} (v - v_1')^2 \quad (40, 41)$$

Appendix IV : glossary of symbols

For convenience of the reader, we list below brief explanations of the main symbols used in this paper.

italic except what marked

h

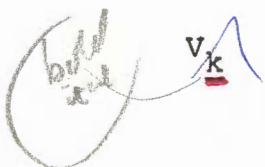
bold ital

200

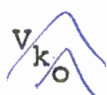
fig 1

- em # after longest entry*
A The constant which multiplies $E^{1/3}$ in (51); defined by (60).
- E Electric field.
- e Electronic charge.
- \hbar Planck's constant ($h/2\pi$).
- rem* i Magnitude of the current pulse at the collector, measured at t_5 (see figure 5b).
- \underline{k} Roton wave-vector.
- rem* k_B Boltzmann's constant.
- k_0 Roton parameter representing magnitude of roton wave-vector at the minimum in energy.
- k_1' Magnitude of roton wave-vector which minimizes the right hand side of (3), for single roton emission: hence, the value of k for the roton which is created in critical dissipation.
- k_2' As for k_1' , but referring to two-roton emission, assuming that both the rotons have the same value of k .

- l Length of drift space between G_2 and G_3 of experimental chamber (see figures 5 and 6)
- m Mass of object being drawn through superfluid ^4He
- m_4 ^4He atomic mass
- m_i Effective mass of negative ion
- m_r Roton parameter representing the effective mass of a roton
- P Pressure
- q Roton wave vector.
- R_1 Transition rate for creation of single rotons by moving ion
- R_2 Transition rate for creation of pairs of rotons by moving ion
- r_i Radius of negative ion
- T Temperature
- $T_{k,k}$ The calculated T-matrix for 2-roton emission
- t Time
- t_1, t_6 Times on idealized collector characteristic (see figure 5b)
- V_D Potential difference across drift space $G_2 G_3$



Matrix element coupling ion to single roton of wavevector k .

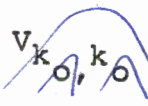


Matrix element coupling ion to single roton at the minimum of roton energy.

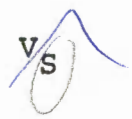


Matrix element coupling ion to pair of rotons with wavevectors k and g .

zeros $\hat{0}$



Matrix element coupling ion to pair of rotons both of which are at the minimum of roton energy.



Transient step in potential applied to field emitter (figure 5b).

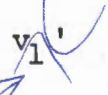


Transient step in potential applied to grid G_1 to open gate (figure 5b).



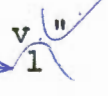
v

Velocity of object through superfluid helium.



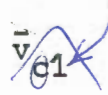
v_1'

Instantaneous critical velocity, given by (9) and approximately by (14), of the object which is required for the emission of one roton (see figure 13a).



v_1''

Instantaneous velocity given by (10) and approximately by (15) of the object immediately after emitting a roton, if it was travelling initially at v_1 (see figure 13a).



\bar{v}_{G_1}

Average velocity of object ($\frac{1}{2}[v_1' + v_1''] \approx v_L$) in critical dissipation (see figure 13b).



v_{e1} Velocity at which ion is travelling, on average, when it emits a roton in supercritical dissipation (see figure 14).

v_{f1} Velocity at which ion travels, on average, immediately after emission of a roton in supercritical dissipation (see figure 14).

\bar{v}_1 Average velocity ($= \frac{1}{2}[v_{e1} + v_{f1}]$) of ion when supercritical dissipation occurs through emission of single rotons: what one would measure in an experiment.

Δv_1 Increment of velocity lost by the ion ($= v_{e1} - v_{f1}$), on average, in creating a roton in supercritical dissipation: given to a good approximation by (20).

v_2' Instantaneous critical velocity, given by (35) and approximately by (39) of the object which is required for the emission of a pair of rotons (see figure 13a).

v_2'' Instantaneous velocity, given by (36) and approximately by (40), of the object immediately after emitting a pair of rotons, if it was travelling initially at v_2' (see figure 13a).

\bar{v}_2 Average velocity of the object ($= \frac{1}{2}[v_2' + v_2''] = v_L$) in critical dissipation (see figure 13b).

- v_{e2} Velocity at which ion is travelling, on average, when it emits a pair of rotons in supercritical dissipation (see figure 16)
- v_{f2} Velocity at which ion travels, on average, immediately after emission of a pair of rotons in supercritical dissipation (see figure 16)
- \bar{v}_2 Average velocity of ion ($=\frac{1}{2}[v_{e2} + v_{f2}]$) when supercritical dissipation occurs through emission of pairs of rotons: what one would measure in an experiment.
- Δv_2 Increment of velocity lost by ion ($= v_{e2} - v_{f2}$), on average, in creating a pair of rotons: given to a good approximation by (45)
- v_{ub} Takken's (1970) estimate of the upper bound on the velocity of an object moving through superfluid ^4He , given by (8)
- v_t Random thermal velocity
- α Coefficient in the single-roton transition rate equation (18), defined by (19)
- β Coefficient in the two-roton transition rate equation (43), defined by (44)
- Δ Roton parameter representing the roton minimum energy

ϵ Energy of a roton, given by (5).

ϵ_1' The roton energy given by substituting k_1' in (5);

hence, the energy of a roton emitted in

(single-roton critical dissipation,

ϵ_2' As for ϵ_1' , but referring to two-roton emission, assuming that both rotons have the same energy

θ The unit step function.

μ Ionic mobility ($= \bar{v}/E$ for small values of \bar{v}).

ν Creation rate of quantised vortex rings by moving ion.

ρ Density of liquid ^4He .

τ_1 Period of time which elapses, on average, before

a roton is emitted in supercritical dissipation:

if $v_{f1} < v_1'$, it is measured from the moment when the ion accelerates through v_1' ; and, if $v_{f1} > v_1'$, it is measured from the time at which the preceding emission event occurred.

τ_2 Period of time which elapses, on average, before

a pair of rotons is created in supercritical dissipation: if $v_{f2} < v_2'$, it is measured from the moment when the ion accelerates through v_2' ; and, if $v_{f2} > v_2'$, it is measured from the time at which the preceding emission event occurred.

τ_D Time for an ion to traverse the drift space between G_2 and G_3 (figure 5a): usually determined by measuring $(t_5 - t_2)$ (figure 5b).

- τ_e Rise time of the electronic circuitry used in detecting the current pulse reaching the collector, (C) (figure 5a).
- Ω Volume within which the roton creation events occur.

Calc

57 VAF
U.S. (2)
NORTH

References

x Allum, D.R., McClintock, P.V.E., & Phillips, A. 1975a
 Proc. 14th. Int. Conf. on Low Temperature Phys. (eds
 M. Krusius and M. Vuorio), vol. 1., pp. 248-51. Amsterdam,
 and Oxford: North-Holland Publishing Company.

x Allum, D.R., McClintock, P.V.E., & Phillips, A. 1975b
 Phys. Lett. (to be published).

Bowley, R.M. 1976 J. Low Temperature Phys. (to be published).

Bowley, R.M. & Sheard, F.W. 1975 Proc. 14th. Int. Conf.
on Low Temperature Phys. (eds M. Krusius & M. Vuorio),
 vol. 1., pp. 165-8. Amsterdam, and Oxford: North-Holland
 Publishing Company.

Brody, B. 1975 Phys. Rev. B 11, 170-7.

Dahm, A.J. 1969 Phys. Rev. 180, 259-62.

Donnelly, R.J. 1972 Phys. Lett. 39A, 221-2.

Fetter, A.L. 1975 In The Physics of Liquid and Solid Helium
 (eds K.H. Benneman & J.B. Ketterson). New York; to be
 published: J. Wiley and Sons Inc. (to be published).

Harrison, S.J. & Mendelssohn, K. 1974 Proc. 13th. Int. Conf.
on Low Temperature Phys. (eds K.D. Timmerhaus, W.J. O'Sullivan

3 on
proof



and E.F. Hammel), vol. 1, p/p. 298-301. New York, and London: Plenum Press.

Henshaw, D.G. / and Woods, A.D.B. 1961 Proc. 7th. Int. Conf. on Low Temperature Phys. (eds G.M. Graham and A.C. Hollis-Hallett), p/p. 539-⁵42. Amsterdam: North-Holland Publishing Company.

Hess, G.B. 1974 Proc. 13th. Int. Conf. on Low Temperature Phys. (eds K.D. Timmerhaus, W.J. O'Sullivan and E.F. Hammel), vol. 1, p/p. 302-³⁰6. New York and London: Plenum Press.

Kuper, C.G. 1961 Phys. Rev. 122, 1007-11.

Keller, W.E. / 1969 Helium-three and Helium-four. New York: Plenum Press.

Landau, L.D. 1941 J. Phys. Moscow 5, 71-90. (Reprinted in Khalatnikov, I.M. 1965 Introduction to the Theory of Superfluidity, p/p. 185-204. New York: W.A. Benjamin).

Landau, L.D. 1947 J. Phys. Moscow 11, 91-2. (Reprinted in Khalatnikov, I.M. 1965 Introduction to the Theory of Superfluidity, p/p. 205-⁷⁰6. New York: W.A. Benjamin).

Meyer, L. / and Reif, F. 1961 Phys. Rev. 123, 727-⁷31.

Neeper, D.A. 1968 Phys. Rev. Lett. 21, 274-5. ²⁷

Neeper, D.A. and Meyer, L. 1969 Phys. Rev. 182, 223-34. ²

Ostermeier, R.M. 1973 Phys. Rev. A8, 514-⁵29.

new

Ostermeier, R.M., Yarmchuk, E.J. & Glaberson, W.I. 1975 Phys. Rev. Lett. 35, 957-60.

Phillips, A. & McClintock, P.V.E. 1973 Phys. Lett. 46A, 109-10.

Phillips, A. & McClintock, P.V.E. 1974 Phys. Rev. Lett. 33, 1468-71.

Phillips, A. & McClintock, P.V.E. 1975 Phil. Trans. Roy. Soc. A278, 271-310.

Poitrenaud, J. & Williams, F.I.B. 1972 Phys. Rev. Lett. 29, 1230-2; and erratum, 1974 Phys. Rev. Lett. 32, 1213.

Rayfield, G.W. 1966 Phys. Rev. Lett. 16, 934-6.

Rayfield, G.W. 1968 Phys. Rev. 168, 222-23.

Reif, F. & Meyer, L. 1960 Phys. Rev. 119, 1164-1173.

Robertson, S.H. & Seidman, D.N. 1968 J. Sci. Instrum. (J. Phys. E.) (GB) 1, 1244-5.

Schwarz, K.W. 1972 Phys. Rev. A6, 837-44.

Schwarz, K.W. 1975 Advances in Chem. Phys. 33, 1-49.

Springett, B.E., Cohen, M.H. & Jortner, J. 1967 Phys. Rev. 159, 183.

Takken, E.H. 1970 Phys. Rev. A1, 1220-39.

Wilks, J. 1967 The Properties of Liquid and Solid Helium. Oxford: Clarendon Press.

Spindars

~~Rules~~

of rules

Pulse	E (kV m^{-1})	N	$(i_c / \text{div}) / nA$
a <i>? it's correct</i>	50	1	0.625 <i>low dec</i>
b	50	2048	0.625
c	65	1	2.50
d	65	128	2.50
e	100	64	12.5
f	200	32	25.0

ts

Table 1.

Experimental conditions under which each of the pulses illustrated in figure 8 was recorded.

Figure captions

bold ital

FIGURE

W

1. An object travelling (a) with initial velocity v_e can reduce its kinetic energy by, as shown in (b), creating an excitation of energy ϵ and momentum $\hbar k$ in the fluid: it moves finally at the smaller velocity v_f .

FIGURE

W

2. The dispersion curve for excitations in superfluid ^4He at a temperature of 1.1K and under a pressure of 25.3 atmospheres (after Henshaw & Woods, 1961): the energy ϵ of an excitation is plotted against the magnitude of its wave-vector k . Excitations near the local minimum are known as rotons. As demonstrated by (6), (4) is satisfied by rotons at the point where a straight line drawn from the origin makes a tangent with the curve, and the gradient of this line therefore represents the Landau critical velocity for roton creation, v_L .

low dec

FIGURE

W

3. The drag exerted by the superfluid upon a moving object as a function of its velocity according to Landau. Taken ⁽¹⁹⁷⁰⁾ / predicted that, for experimentally feasible measurements of negative ion characteristics, curve (a) would be followed; but curves such as (b) or (c) would be equally consistent with Landau's theory, which merely predicts the absence of drag for velocities below v_L .

FIGURE

W

4. Field emission characteristics in superfluid ^4He under pressure. In (a) the current i from an emitter at 3.0kV is plotted as a function of pressure at a fixed temperature, and is seen to increase rapidly above $10 \times 10^5 \text{ Pa}$.

In (b) the currents from an emitter at 2.0kV are plotted against temperature T for two pressures P: the current at 25×10^5 Pa is considerably larger than at 10^5 Pa and is temperature independent below 0.5K.

FIGURE

5. The single-pulse time of flight technique. The main components of the electrode structure are shown diagrammatically in (a). In (b) are sketched, as functions of time t: the transient negative potentials V_S (≈ 1.5 kV) and V_{G_1} (≈ 50 V) applied respectively to the field emission source S and to the grid G_1 ; and the resultant negative current i_C which in practice is found to be induced in the collecting electrode C.

FIGURE

6. The experimental chamber, slightly modified so as to appear in a single vertical section. The main components were all cylindrically symmetrical. (a), Chamber body, which was flattened on one face to ensure good thermal contact with the ^3He pot; (b), (c), brass endplates, bolted to chamber body over indium 'o' rings; (d), tungsten field emitter, spot-welded to nickel wire; (e), nylon holder for field emitter; (f), brass back-plate of emission chamber; (g), brass grid-support-ring, which was a tight fit in back-plate; (h), grid G_1 ; (i) grid G_2 ; (j), brass guard rings to maintain uniform electric fields between G_2 and G_3 ; (k), nylon insulating rings (l) Frisch screening grid, G_3 ; (m), nylon tube to align electrode stack; (n), nylon sleeve to insulate electrode connecting

wires from chamber body; (o) brass collector; (p) brass guard ring for collector; (q) nylon insulator; (r) nylon body of insert which was also drilled to accept a carbon resistance thermometer (not shown); (s) one of the three spring-loaded bolts securing insert to endplate; (t) one of two 2-pin metal-glass seals carrying electrical connections for collector and resistance thermometer; (u) 12-pin metal glass seal carrying electrical connections for the field-emitter, G_1, G_2 , guard rings for the main electric field, and G_3 ; (v) nylon distance piece, bolted very loosely to component (m), which transmitted the force of the springs around the bolts (s), via components (r), (q), (p) and (t), to the electrode stack inside (m).

FIGURE

7. Block diagram of the electrical circuit used in making the time of flight measurements. The components enclosed by the dashed line are all at liquid helium temperature.
8. Typical data recorded for a temperature of $0.3K$ and a pressure of $25 \times 10^{-5} Pa$: the current i_c appearing at the collector is plotted (with arbitrary origin) as a function of time t , measured from the moment at which the gate was opened. The transient negative potential V_s applied to the emitter was $1.5kV$, and that V_{G_1} applied to the first grid was $30V$; the stopping potential, when the gate was shut, was $10V$. The emitter switching-off transient (Y of figure 5b) occurred near $t=500\mu s$, and so is not visible in these results. For each of the individual pulses illustrated in the figure, the electric field E within the drift space, the number N of signals averaged, and the current represented by one division of the ordinate axis are given in table 1.

FIGURE

9. Experimental values of the ionic drift velocity \bar{v} as a function of electric field E , showing the effects of (a) changing the pressure P and (b) changing the temperature T .

repeat
k
oo

10. Dependence of the pulse height i_c at the collector upon the electric field E between G_2 and G_3 , while keeping all other parameters constant, for two temperatures T . Both sets of data were recorded with a pressure of 25×10^5 Pa.

k
oo

11. The drag on an ion moving through superfluid ^4He at 0.35K , as a function of the average ionic velocity \bar{v} . For comparison, the equivalent plot for an ion moving through normal (non-superfluid) ^4He at 4.0K is also shown, emphasizing the qualitative difference which exists between the two cases. It is clear that drag in the superfluid sets in abruptly at a critical velocity which is very close to the critical velocity for roton creation, v_L , predicted by Landau.

k
oo

12. Critical dissipation for an object being drawn by a constant force through superfluid ^4He : its instantaneous velocity v is plotted as a function of time t .

(a) Whenever the object reaches a critical velocity v_1' given by (9) it emits a roton, dropping to the lower velocity v_1'' given by (10) before accelerating once again to repeat the process. Its average velocity \bar{v}_{c1} is given by (11) and, as will be seen in figure 13(b), is

oo

within 1% of v_L unless the object has a mass less than three ^4He atomic masses.

(b) If, on the other hand, dissipation occurred through two-roton emission events, then the amplitude and period of the waveform would, as discussed in § 4(d), be approximately doubled: simultaneous emission of two rotors would occur every time the object reached a critical velocity v_2' given by (35); its final velocity would be v_2'' given by (36); and its average velocity \bar{v}_{c2} , given by (37), will be seen in figure 13(b) to be within 1% of v_L , provided that the object has a mass greater than six ^4He atomic masses.

FIGURE

13. Critical dissipation: influence of the mass m of the moving object, determined by solving (13) and (38), where m_4 is the ^4He atomic mass.

(a) Plots of the critical instantaneous velocities v_1' and v_2' required respectively for single-roton and two-roton emission events, and of the consequent final velocities v_1'' and v_2'' . All four characteristic velocities tend to the Landau critical velocity v_L in the limit of large mass.

(b) The resultant average velocities \bar{v}_{c1} and \bar{v}_{c2} which would be measured experimentally for critical dissipation through single-roton and two-roton emission processes respectively. Except for very light objects, the average velocity remains closely equal to v_L .

14. Supercritical dissipation through single-roton emission. The ionic instantaneous velocity v is plotted

repeat

as a function of time t : (a) for relatively weak electric fields \underline{E} , such that the average final ionic velocity \underline{v}_{f1} is less than the critical instantaneous velocity \underline{v}_1' required for single-roton creation; (b) for stronger electric fields such that $\underline{v}_{f1} > \underline{v}_1'$. It is assumed that, for any given value of \underline{E} , the ion continues to accelerate for an average time τ_1 after \underline{v}_1' has been exceeded, before the roton is emitted. In (b) it is always the case that $\underline{v} > \underline{v}_1'$, and so τ_1 starts being measured from the moment at which the previous roton was created. As discussed in the text, the amplitude $\frac{1}{2} \Delta v_1$ of the sawtooth may to a good approximation be regarded as independent of \underline{E} .

FIGURE

15. Comparison of some of the experimental data with (26), plotting the measured ionic drift velocity \bar{v} against the (electric field, \underline{E})^{2/3}: an attempt has been made to draw a straight line through the data, intersecting the velocity axis at \underline{v}_L . Even allowing for a possible systematic error of 3% (see § 3(c)) in the values of \bar{v} , the data are clearly inconsistent with (26), which was derived on the assumption of dissipation through single-roton emission.

16. Supercritical dissipation through two-roton emission. The ionic instantaneous velocity \underline{v} is plotted as a function of time t : (a) for relatively weak electric fields \underline{E} , such that the average final ionic velocity \underline{v}_{f2} is less than the critical instantaneous velocity \underline{v}_2' required for creation

of a pair of rotons; (b) for stronger electric fields such that $v_{E/2} > v_2'$.

It is assumed that, for any given value of E , the ion continues to accelerate for an average time τ_2 after v_2' has been exceeded, before the rotons are emitted. In (b) it is always the case that $v > v_2'$, and so τ_2 starts being measured from the moment at which the previous pair of rotons were created.

FIGURE 17. Comparison of some of the experimental data with (51), plotting the measured ionic drift velocity \bar{v} against the (electric field, E)^{1/3}, for two temperatures. The straight lines represent least-squares fits of the data to the equation, treating v_L as though it were an adjustable parameter.

(a) Fitting the 0.35K data within $5 < E < 200 \text{ kV m}^{-1}$ we obtain the line

$$\bar{v} = 46.26 + 0.149 E^{1/3},$$

where \bar{v} is in ms^{-1} and E is in V m^{-1} .

(b) Fitting the 0.45K data within $5 < E < 200 \text{ kV m}^{-1}$ we obtain

$$\bar{v} = 46.10 + 0.146 E^{1/3}.$$


In each case the intercept agrees with the value of v_L calculated from the roton parameters (45.6 ms^{-1}) to well within the possible systematic experimental error of $\pm 3\%$. As discussed in the text, there are theoretical reasons for expecting deviations from the straight line in the limits of high and low electric field. The data are clearly consistent with (51),

W

which was derived on the assumptions of dissipation through two-roton emission, over a wide range of E .


FIGURE

W

18.  A portion of the averaged measurements of the drift velocity \bar{v} plotted against (electric field, E) for large values of E . The full curve represents (51) fitted to the data at smaller values of E , and the dashed curves represent the form taken by (58) for various ionic masses, m_i . The error bars, referring to the average scatter on the unaveraged values of \bar{v} , are to give some indication of the reliability of the data.

(K)

W

19.  The effect of pressure P on the Landau critical velocity for roton creation v_L . The experimental values obtained by fitting data to (51) have been normalized by dividing by the value found for 25×10^5 Pa: this procedure eliminates the effect of the uncertainty of $\pm 3\%$ in their absolute values. The full line has been calculated from accepted values (Donnelly, 1972) of the roton parameters.

1

$(\epsilon/k_B)/K$

2

k/nm^{-1}

3

i/nA

4

$10^{-5} P/Pa$

T/K

5

6

C.V.P. to set, make block

7

i_{c}

8

$t/\mu\text{s}$ - row, upright

$\bar{v}/(\text{m s}^{-1})$

9

$E/(\text{kV m}^{-1})$

i_{c}/mA

10

$E/(\text{kV m}^{-1})$



↑ A9-3

91

$10^{14} \times \text{drag} / N$

11

$\bar{v} / (m s^{-1})$

12

velocity / ($m s^{-1}$)

13

m / m_4

FIG 14: C.O.P. to set, make block

14

$\bar{v} / (m s^{-1})$

15

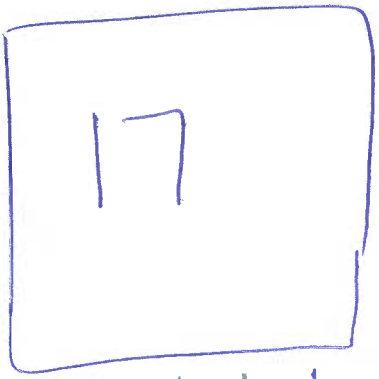
$10^{-3} E^{2/3} / (v m^{-1})^{2/3}$

C.O.P. to set, make block

16

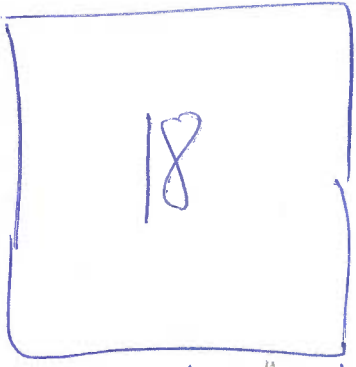


$\bar{v} / (\text{m s}^{-1})$



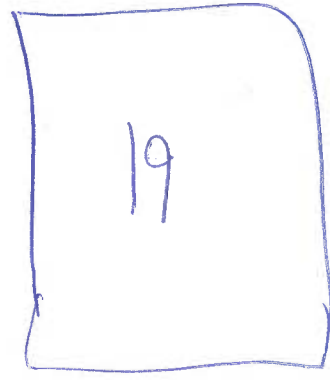
$E^{\frac{1}{2}} / (\text{V m}^{-1})^{\frac{1}{3}}$

$\bar{v} / (\text{m s}^{-1})$



$E^{\frac{1}{2}} / (\text{V m}^{-1})^{\frac{1}{3}}$

$\bar{v}_A (P) / \bar{v}_L (25 \times 10^5)$



$10^{-5} \bar{P} / \text{Pa}$

Figures

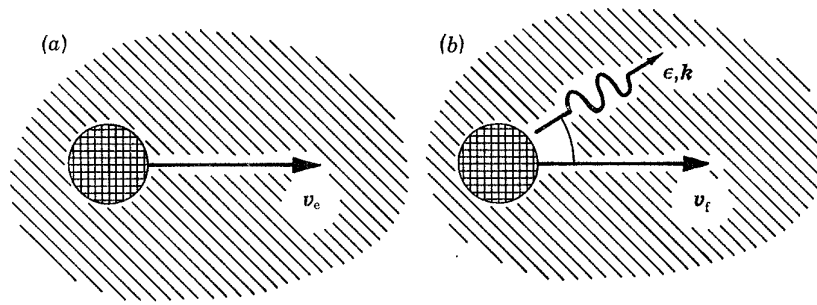


Figure 1:

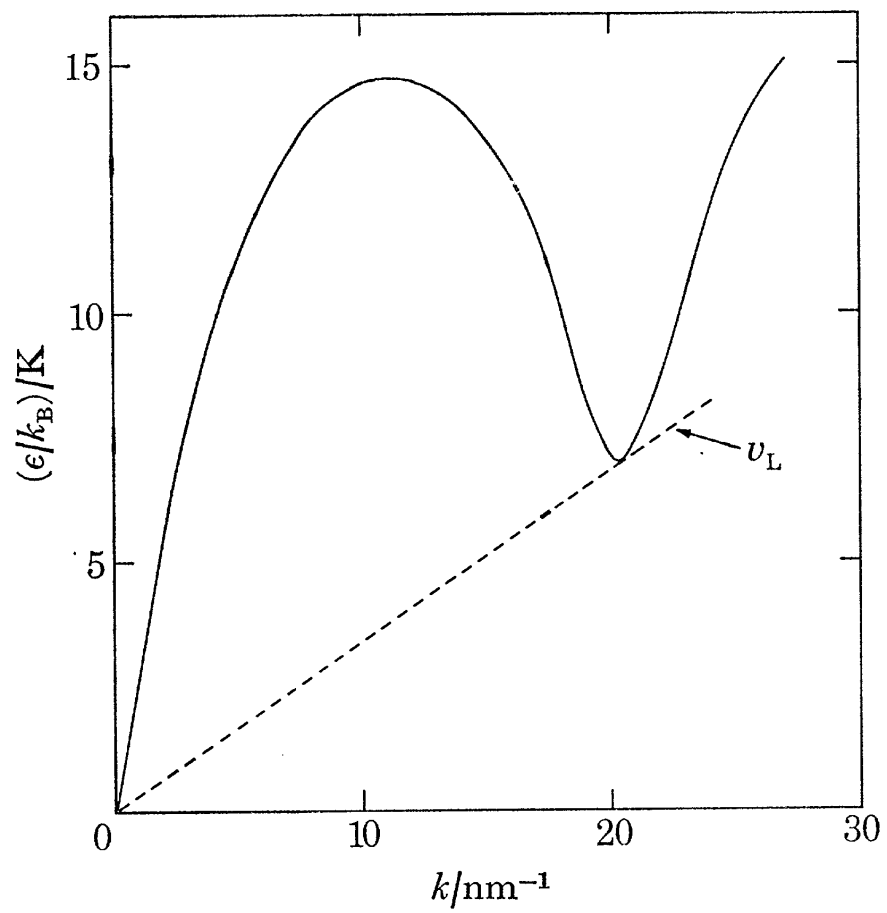


Figure 2:

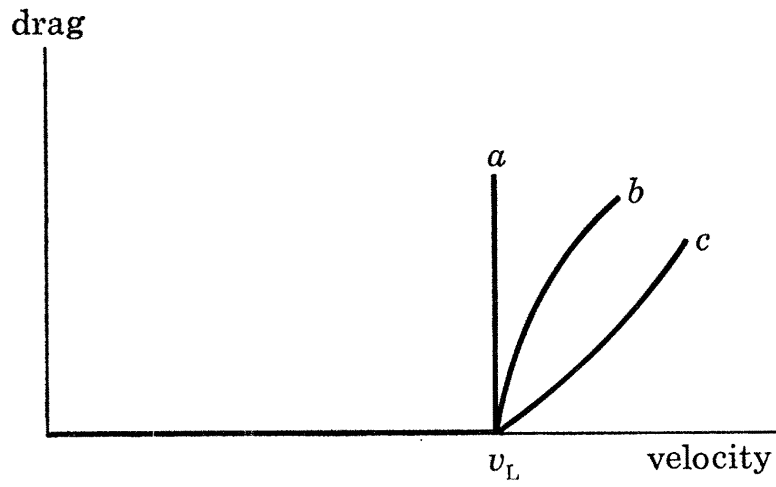


Figure 3:

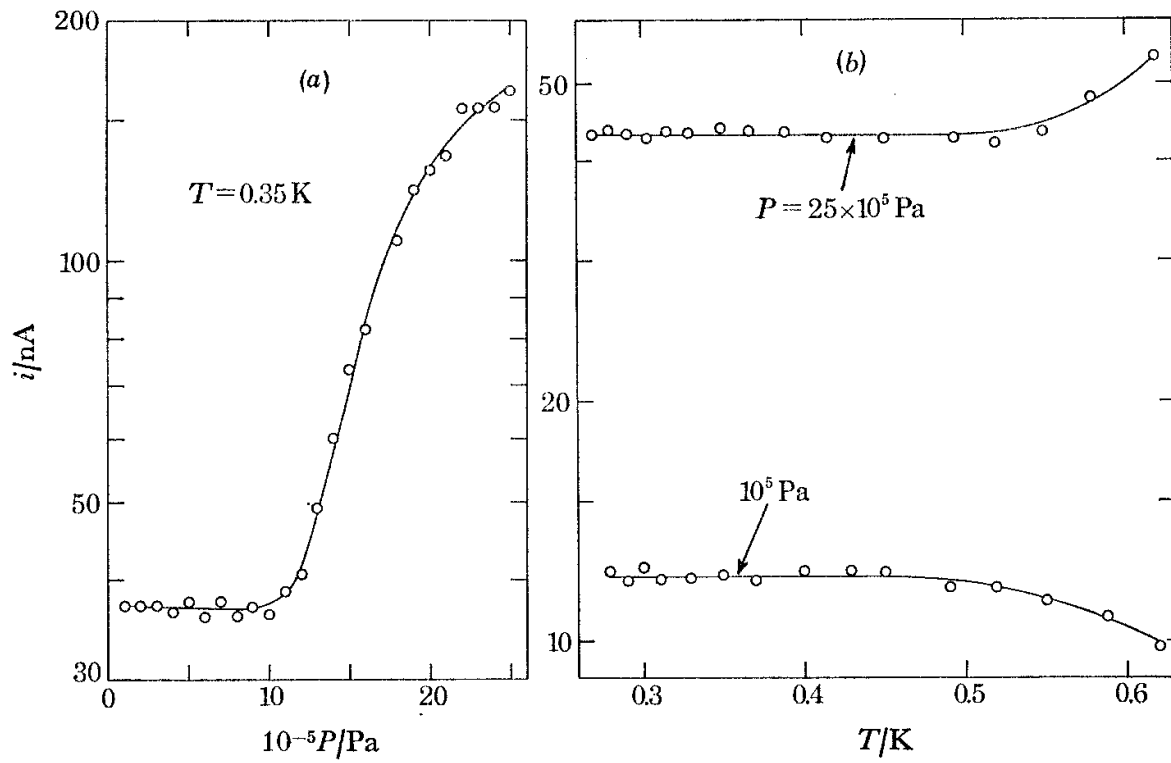
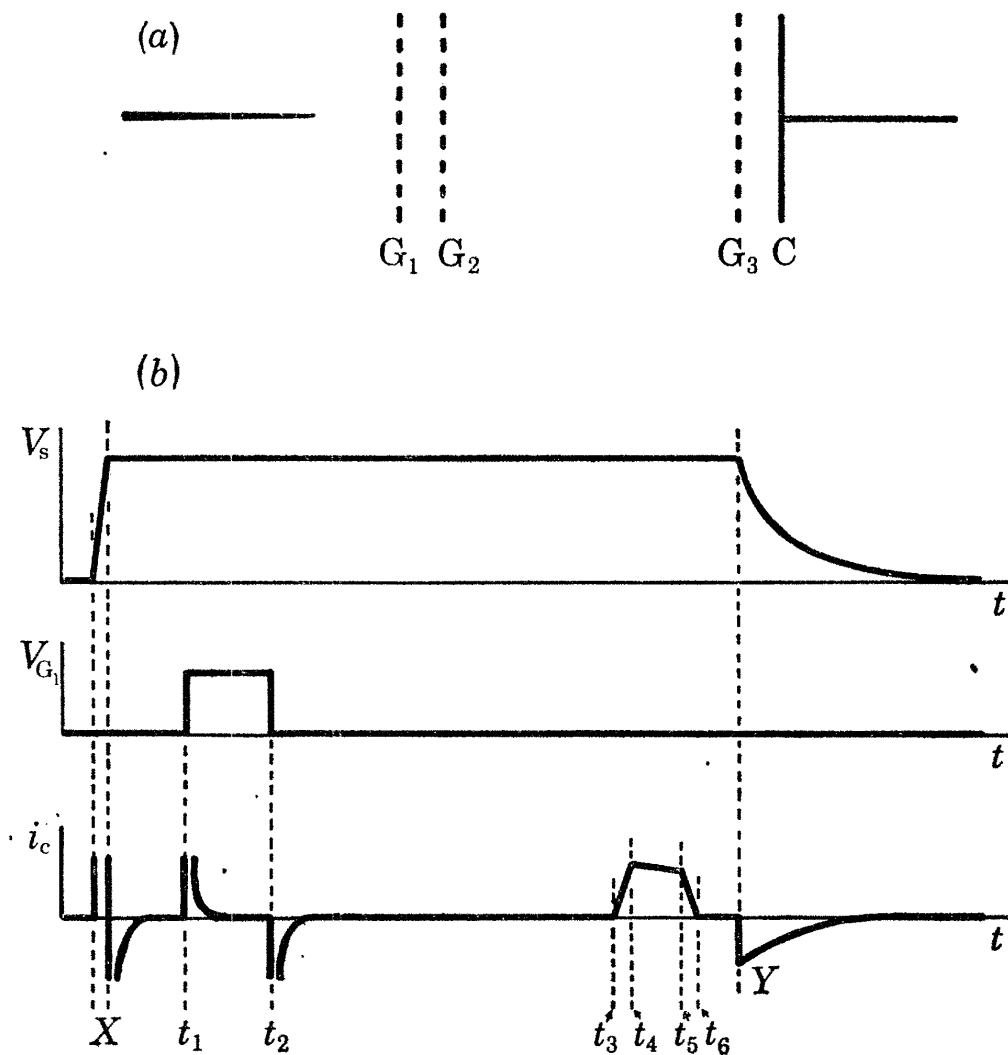


Figure 4:



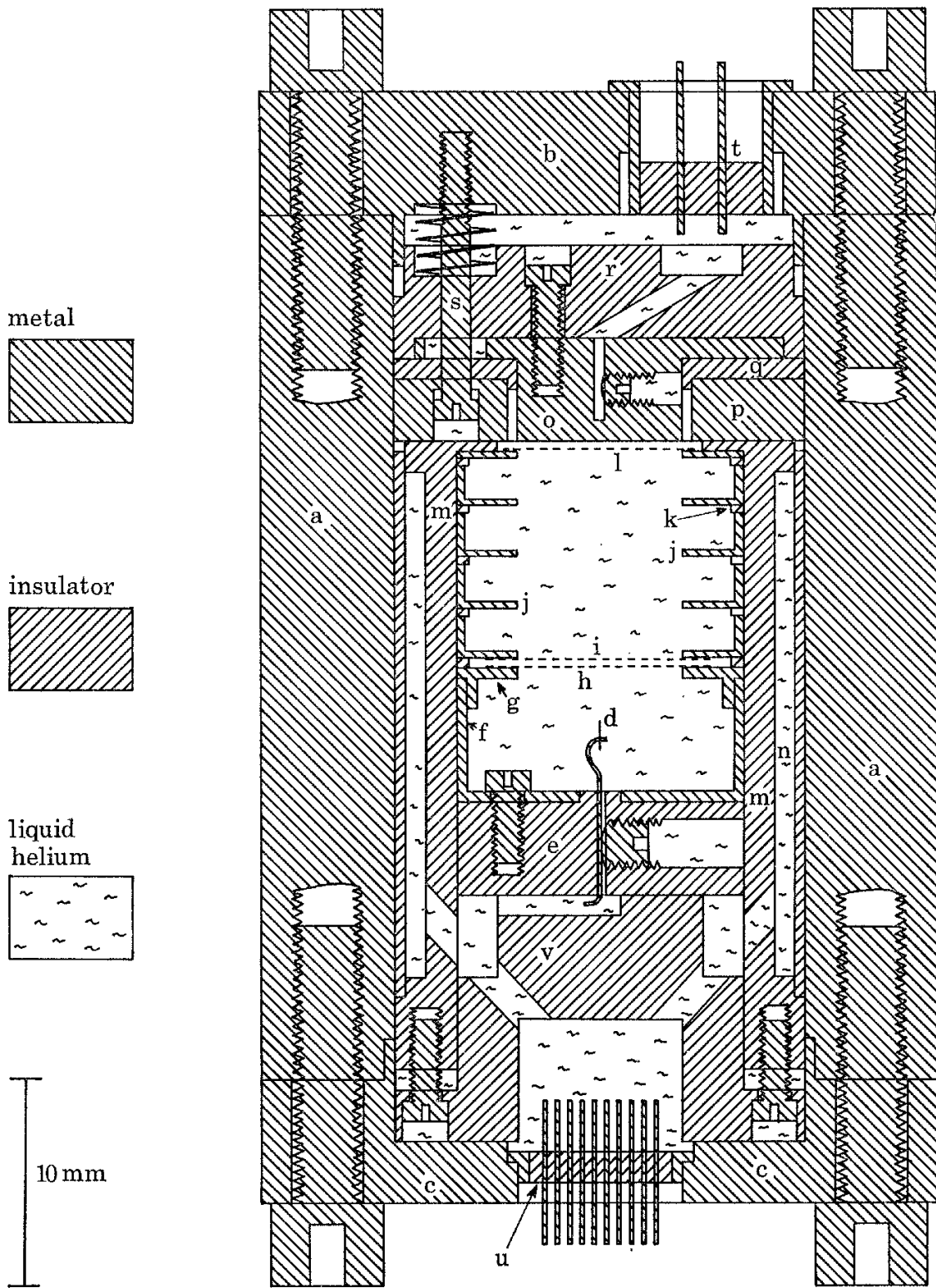


Figure 6:

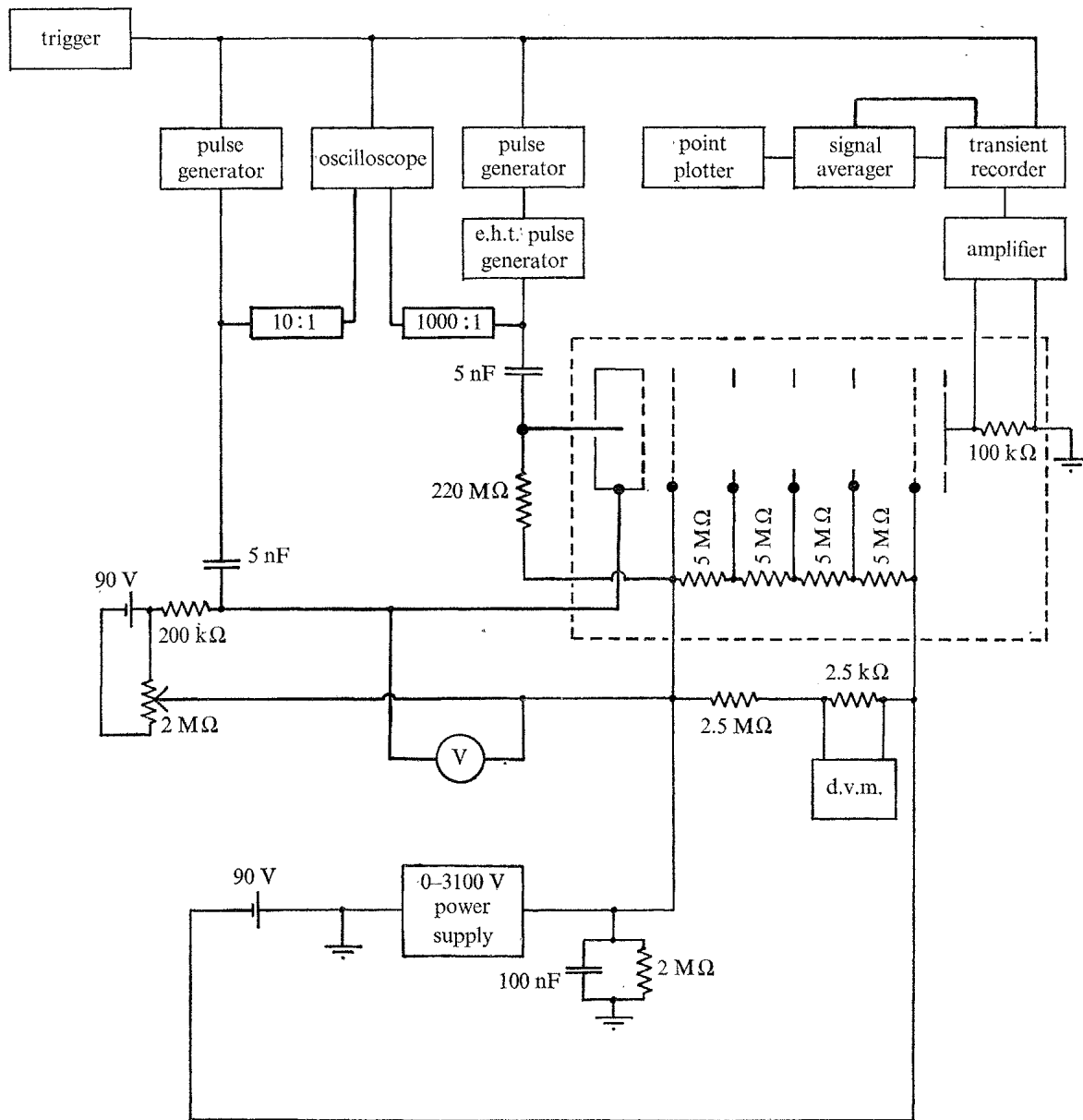


Figure 7:

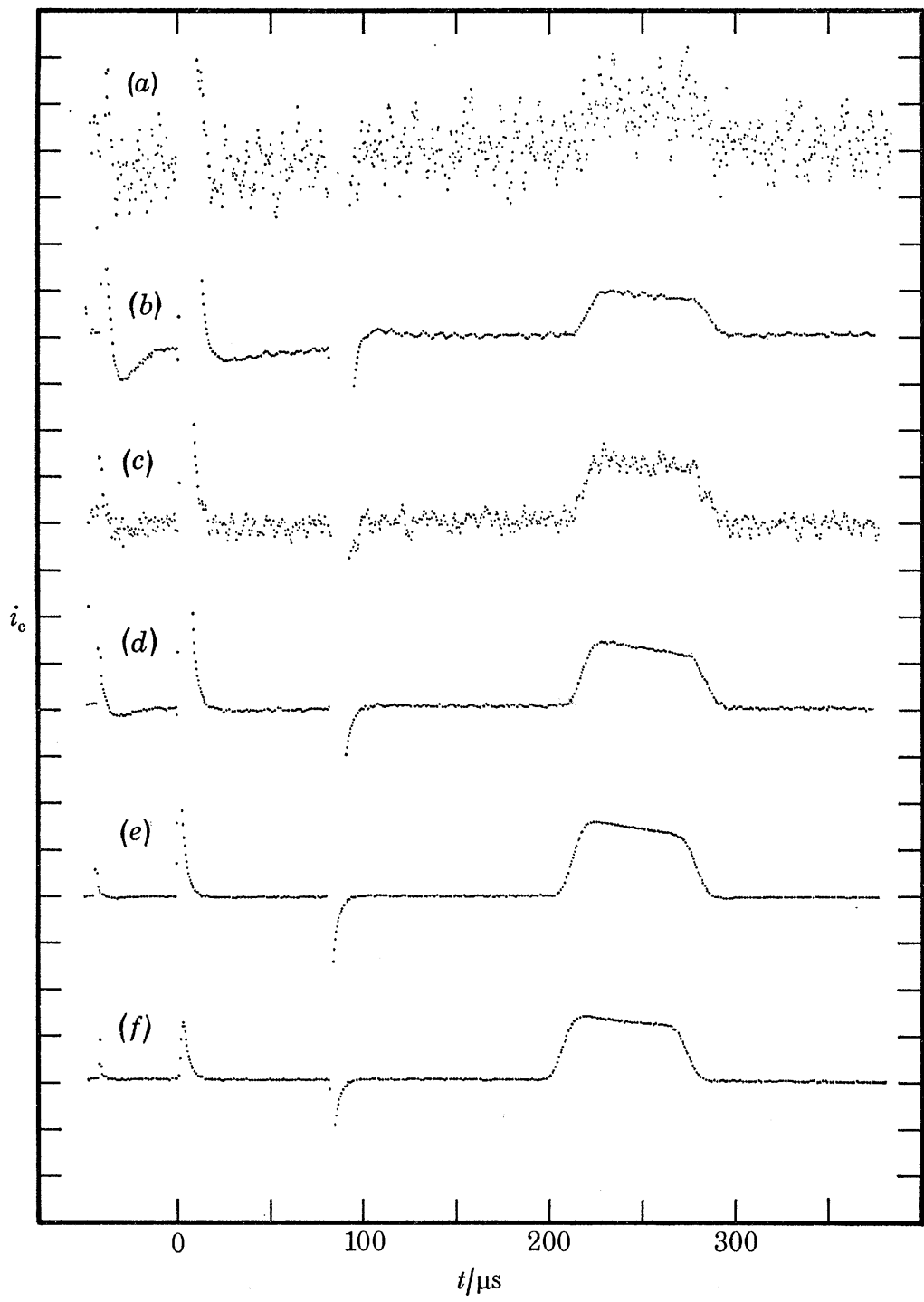


Figure 8:

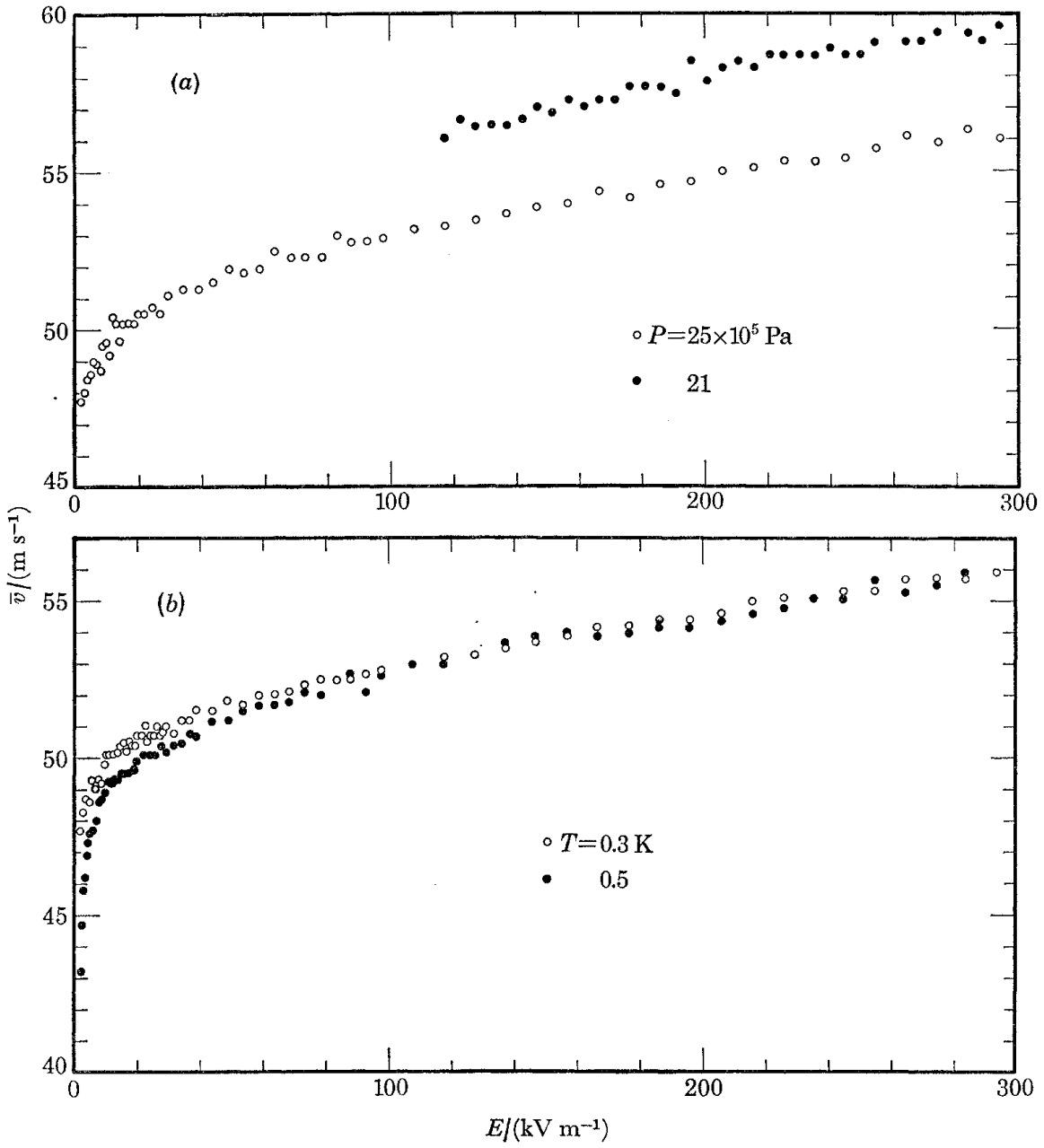


Figure 9:

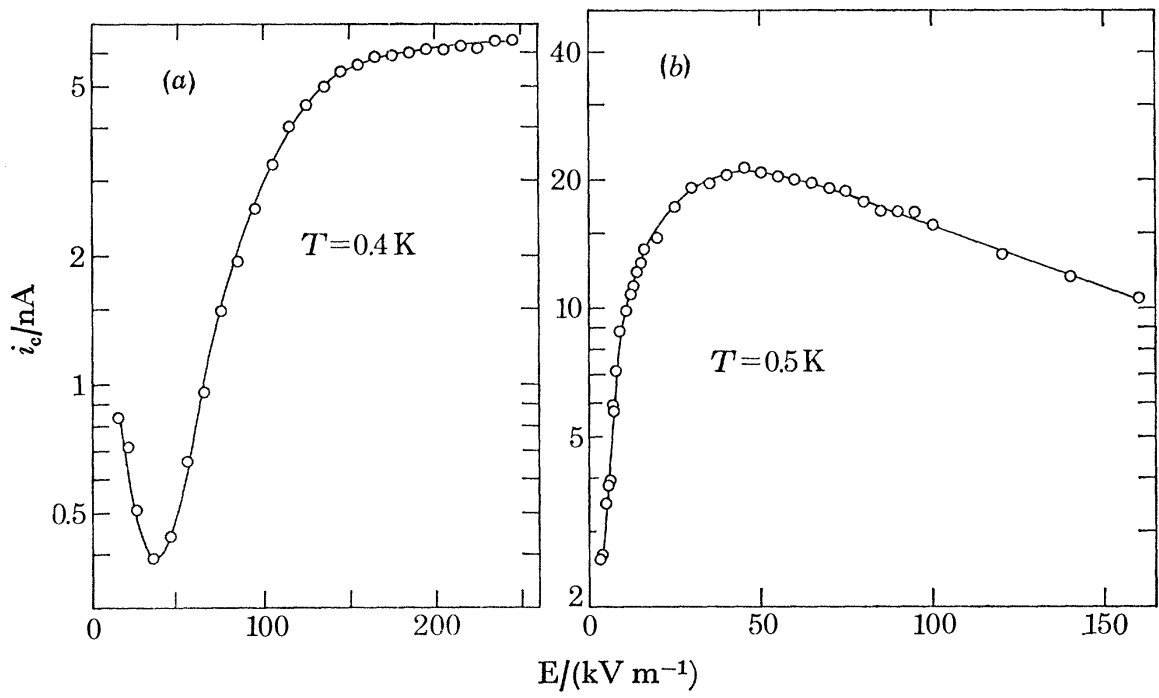


Figure 10:

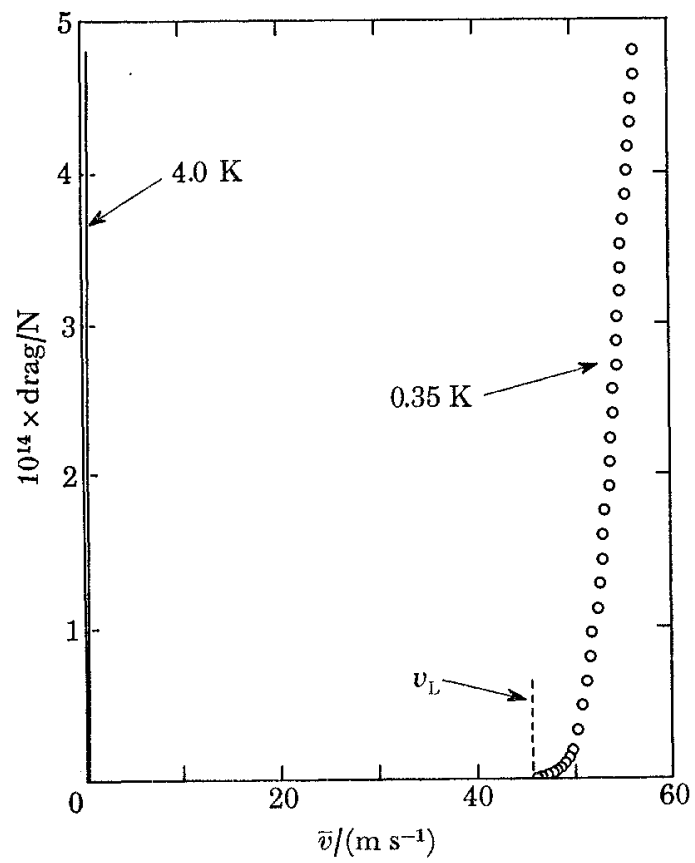


Figure 11:

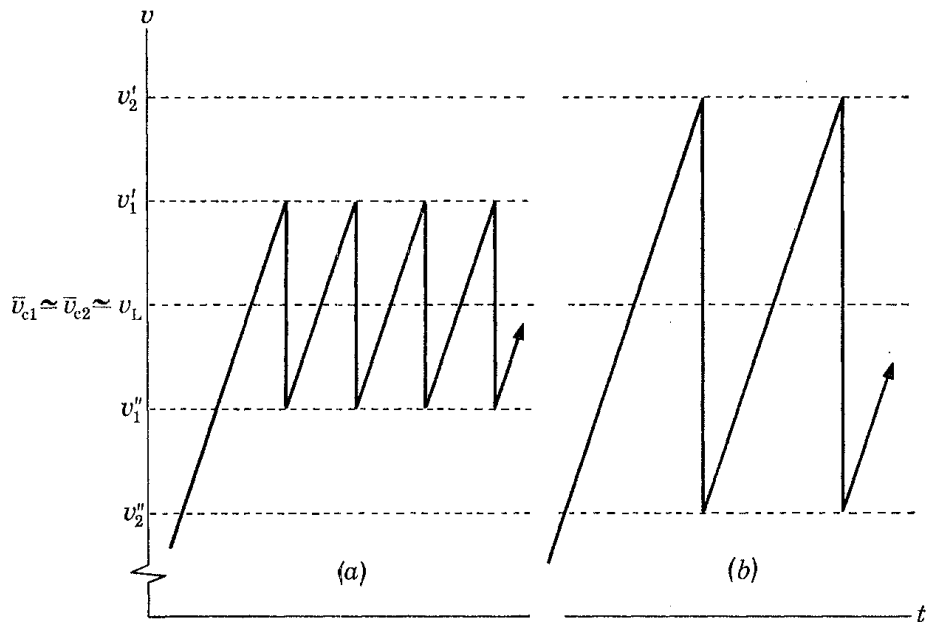


Figure 12:

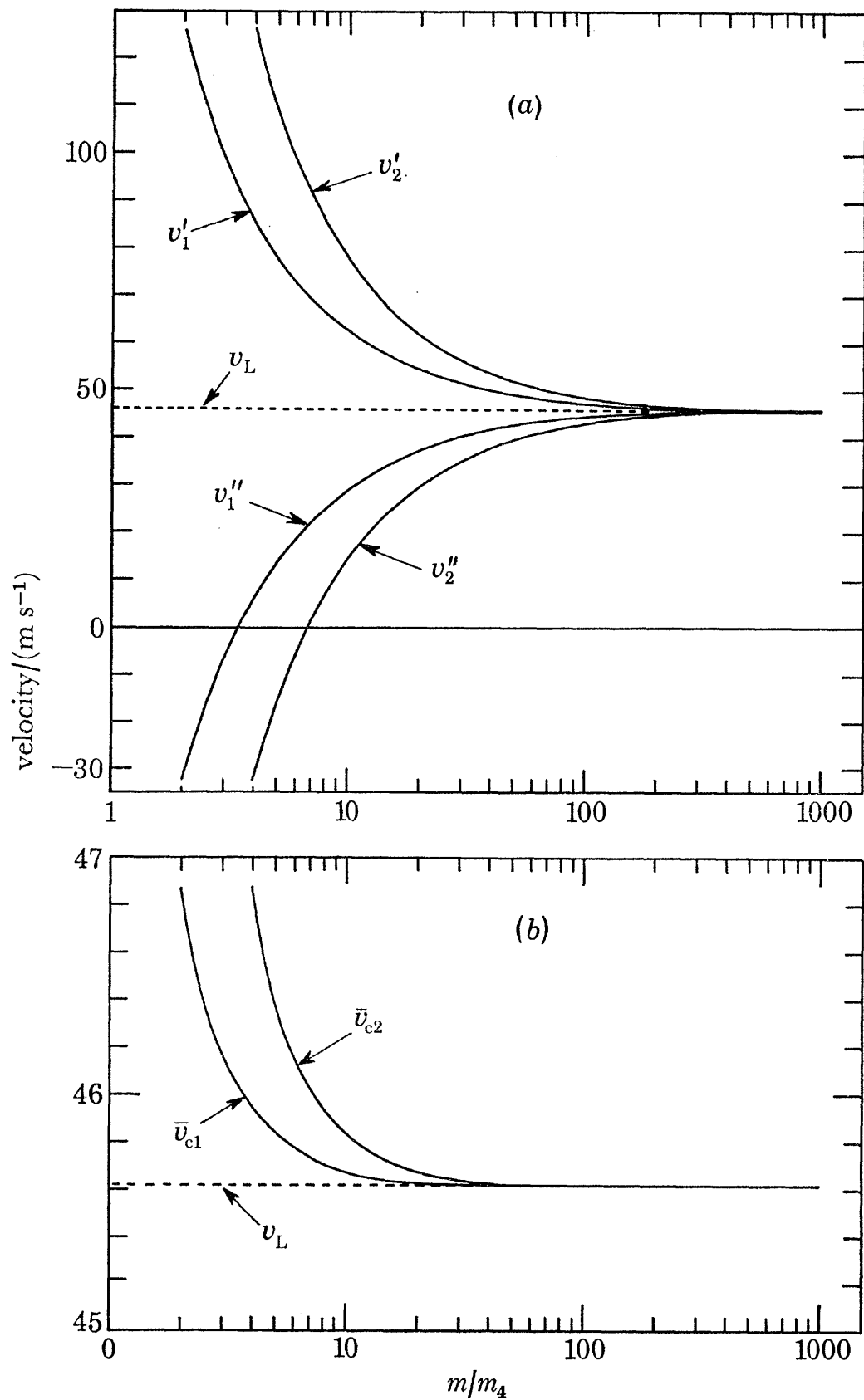


Figure 13:

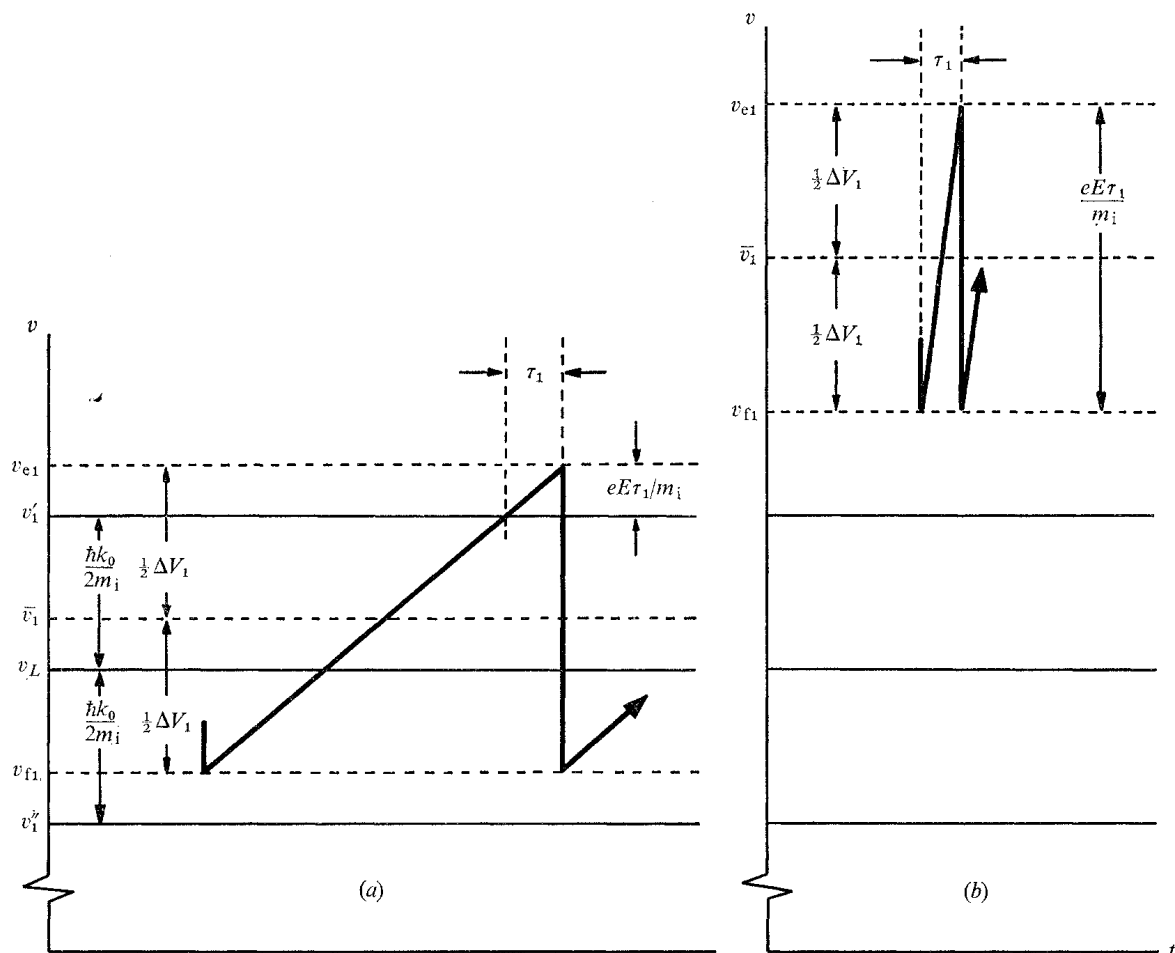


Figure 14:

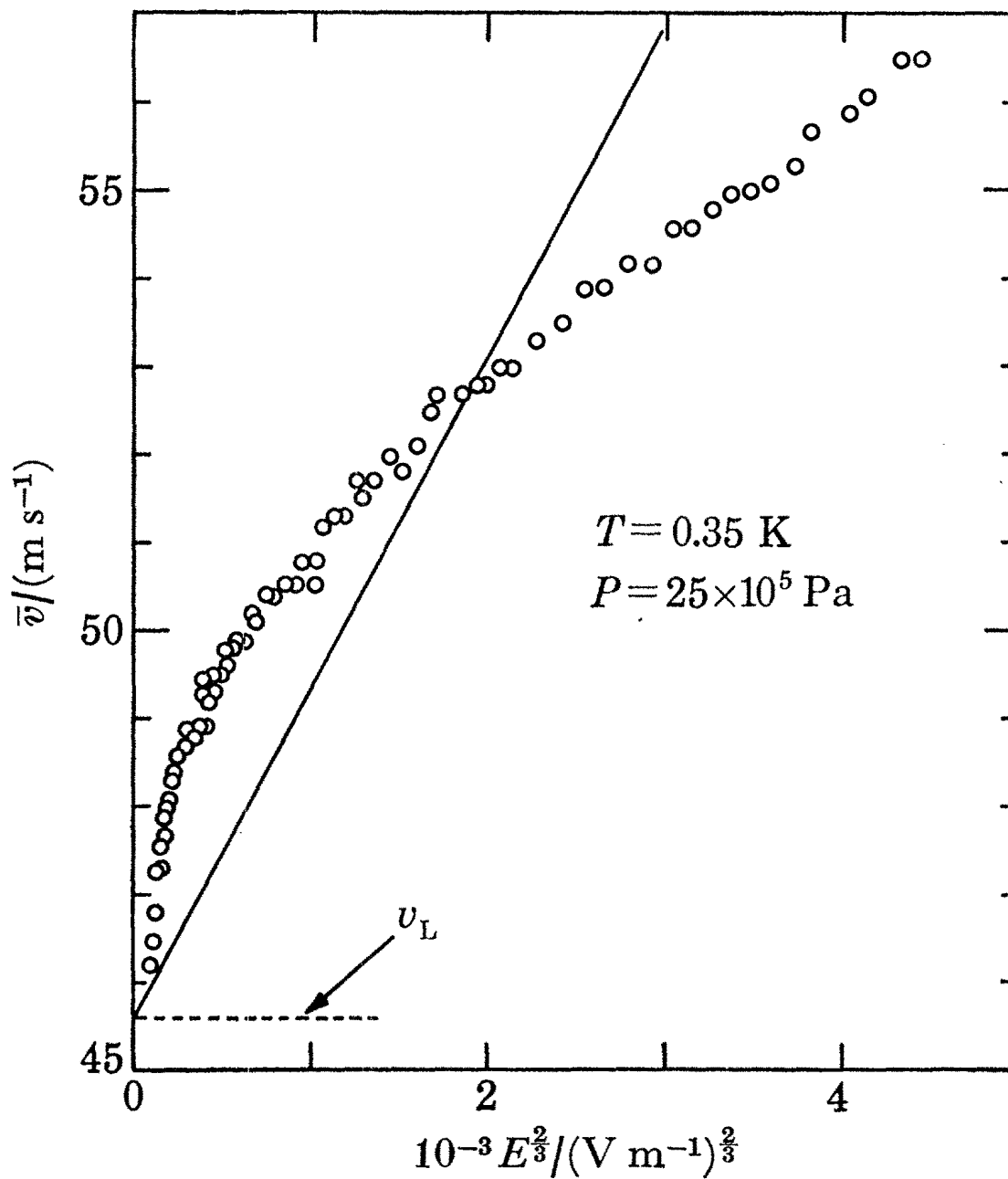


Figure 15:

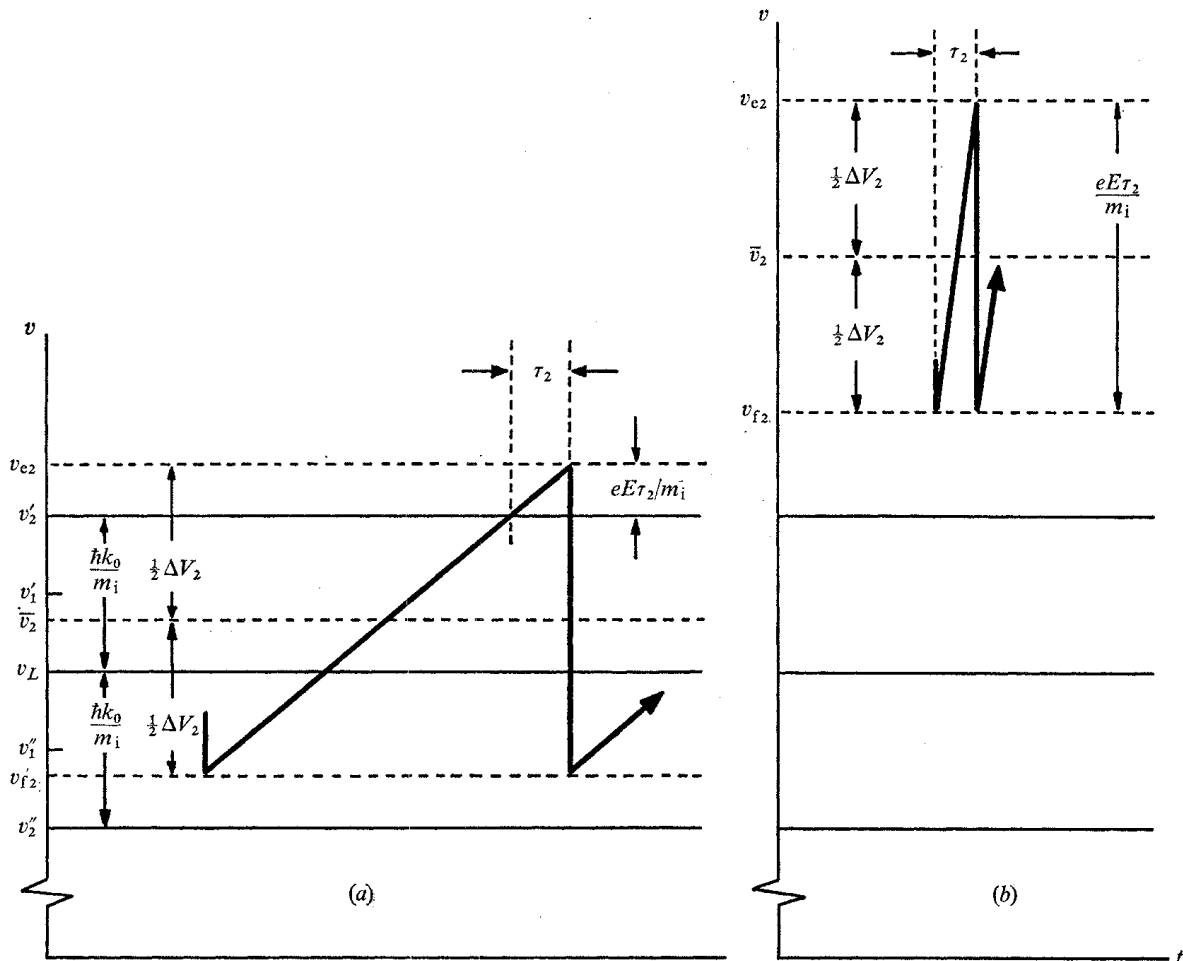


Figure 16:

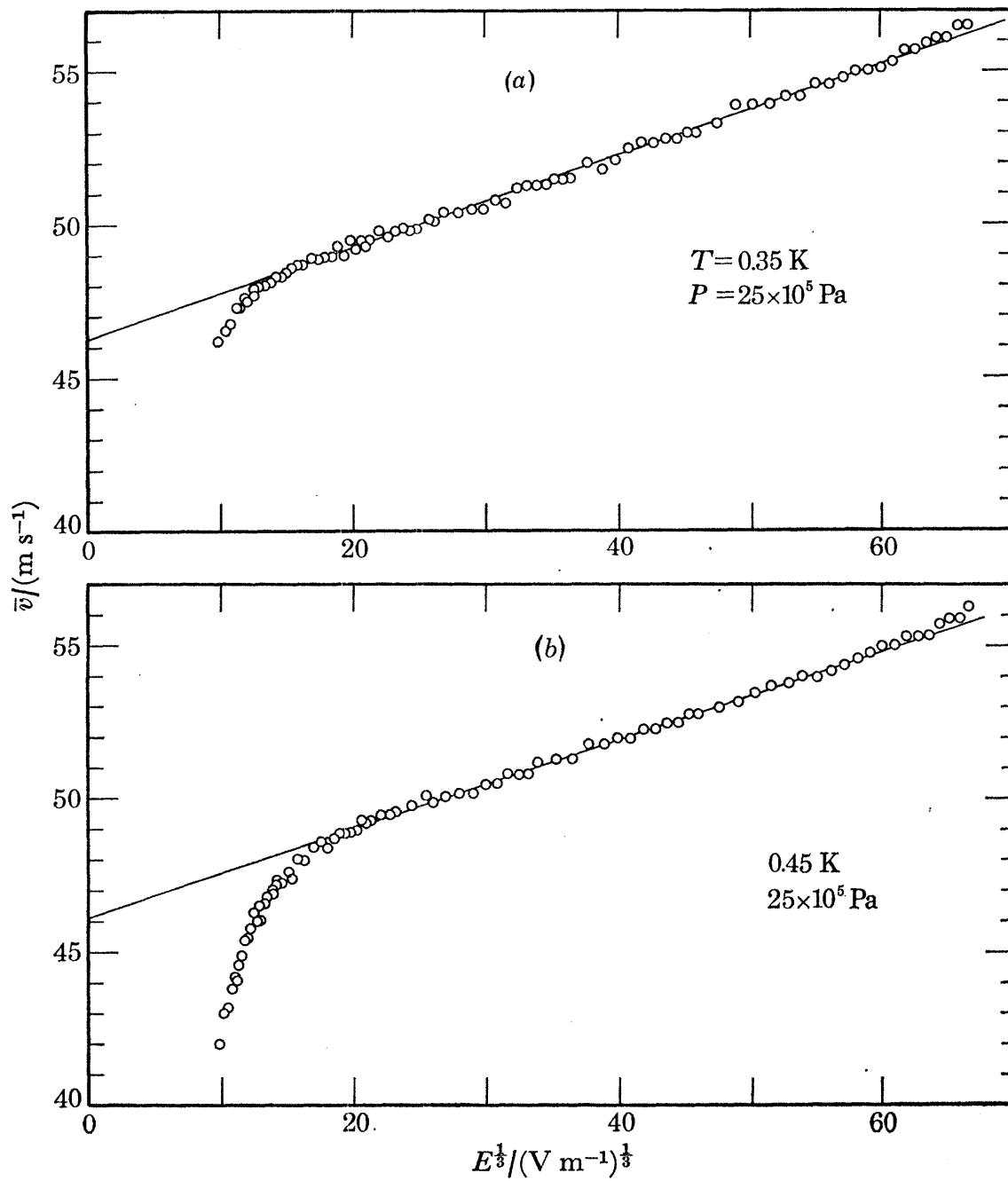


Figure 17:

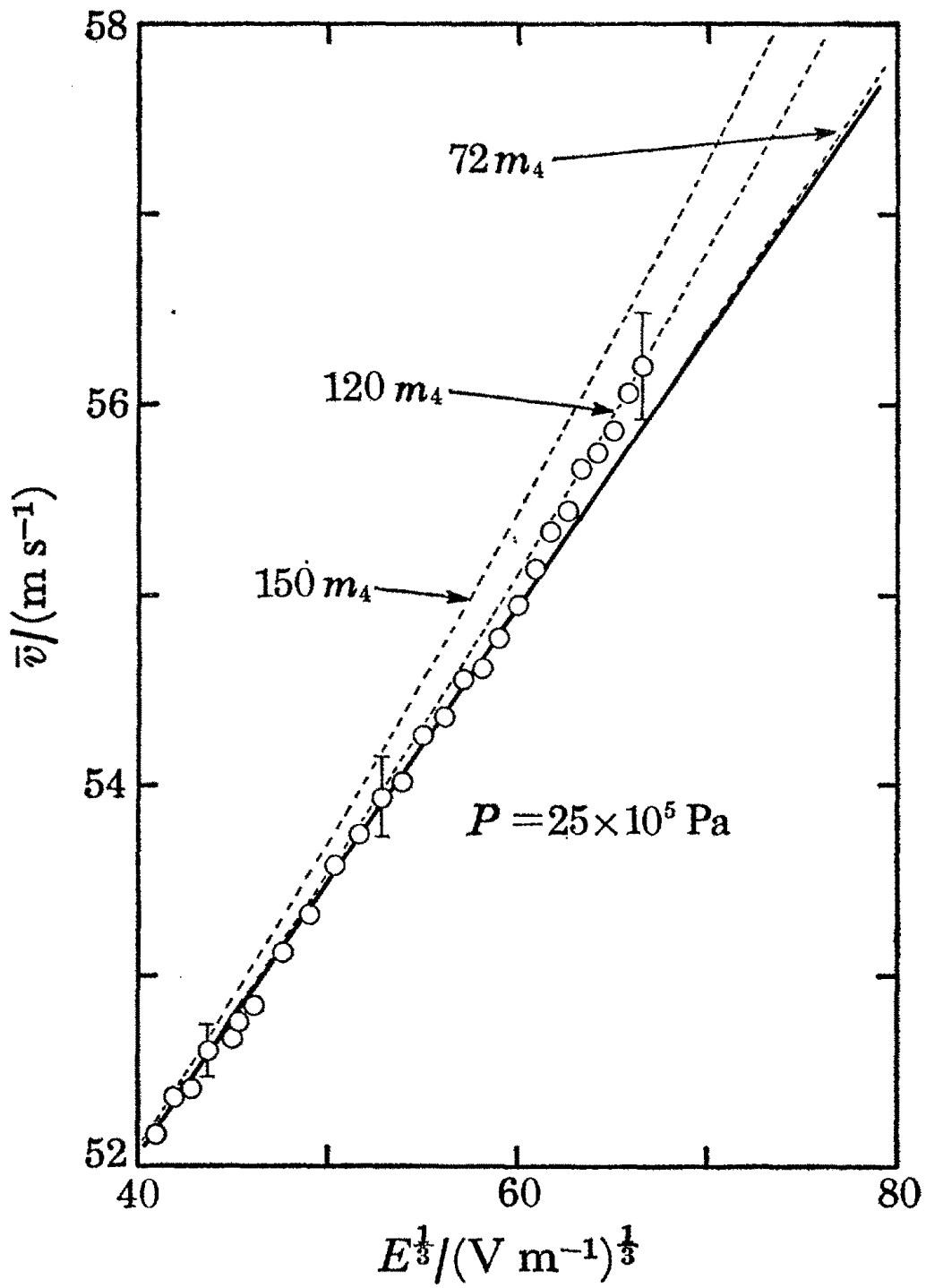


Figure 18: